

# MRI Compatible Motorized 1D Motion Platform

Authors: Kendra Besser, Amber Schneider, Jamie Flogel, Maxwell Naslund, Caspar Uy

## Abstract

### Purpose

Quantitative magnetic resonance imaging (qMRI) is currently limited by motion artifacts due to respiration. An MR safe motion platform that mimics respiratory motion could serve as a qMRI testing and calibration device to address this issue.

### Methods

The platform was developed using accessible parts and fabrication techniques. Tests were run to determine the accuracy and precision of the sinusoidal motion. Additionally, the prototype was tested for MR compatibility.

### Results

Initial testing revealed issues with friction and motor control. Additional rounds of testing suggested low overall period error with mostly acceptable amplitude errors aside from extreme bounds.

### Conclusion

Modifications were made to the design after multiple rounds of preliminary testing. A second round of testing verified the device worked within certain operational bounds. Success of this device would allow for broad usage as a research tool in validating and testing qMRI protocols.

## Introduction

Quantitative magnetic resonance imaging (qMRI) is a new and developing MR technique that measures specified characteristics of the tissues being imaged [1]. Healthcare professionals can utilize qMRIs to assist in many functions, such as detecting tissue characteristic changes over time, diagnosing and monitoring diseases, drug therapy delivery,

and determining drug efficiency [2] [3]. qMRIs map physiological characteristics by correlating the pixel intensity to a measurement of the specified physiological property. Examples of quantifiable characteristics that qMRIs can measure are nuclear magnetic resonance, relaxation times T1 and T2, diffusion and perfusion rates, fat and water fractions, iron fraction, elastic properties of tissue, temperature, chemical composition, and chemical exchange [4]. Figure 1 displays qMRI results for liver fat concentrations.

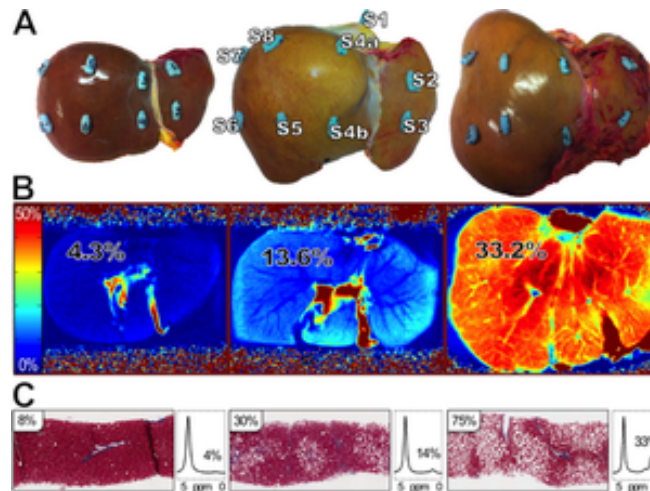


**Figure 1**

Row B shows the qMRI map of liver fat fractions. This image compares a healthy liver (far left) to a steatotic liver (far right). Row C shows the percent fat in each liver with the steatotic liver being 75% composed of fat [3]. The Figure shows how the qMRI map uses different color gradients to represent different fat concentrations across the liver sample.

One major disadvantage of qMRI is their need for precision. Anatomical motion, such as abdominal motion due to respiration, can have an extensive effect on the quality of qMRI results. This motion causes image artifacts, blurring, and ghosting [5]. In an attempt to avoid image distortion, current protocols require patients to practice breath holds during the imaging [5]. This technique requires the patient to hold their breath for 10 to 30 seconds for multiple consecutive periods while being scanned [5]. Figure 2 shows the difference between an MRI image with breath holding and an MRI image without breath holding. Breath hold techniques can be very challenging for pediatric, elderly, severely ill, and sedated patients [6]. Aside from being not feasible for certain populations, the breath holding technique has a short acquisition time to collect data. This short acquisition time leads to decreased quality of imaging with a lower than ideal signal to noise ratio.

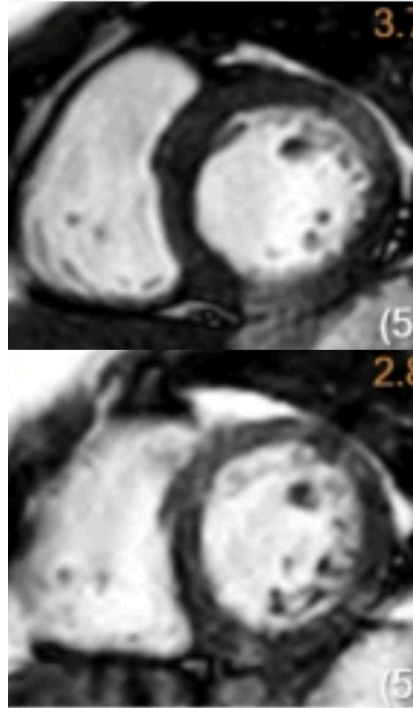


**Figure 2**  
MRI with breath hold (top) and without (bottom) [6]

Before testing tissue samples or scanning patients, qMRIs must be calibrated with precise software and phantoms with known values of the variable being tested [7]. Biological phantoms are also used to test the accuracy and precision of qMRIs and assist in research studies [8]. Specifically, qMRIs of fat concentrations in liver phantoms can assist in the calibration for MRIs to detect and diagnose diseases, such as steatosis [9]. If left untreated steatosis can lead to further liver damage, cancer, or cirrhosis [10]. Unfortunately the static phantoms fall short in accurately capturing the continuous motion due to respiration and digestion. To address this limitation, a specialized MRI-compatible device capable of positioning a phantom and replicating respiratory motion will be developed to enhance the accuracy of qMRI evaluations and eliminate the need for breath holds during scanning [11].

There are a few devices on the market that are being used to produce motion within an MRI for testing of qMRI protocols. In a study done by the Department of Radiology at University of Texas Southwestern Medical Center, researchers developed a one-dimensional MRI compatible motion platform. They used the platform in combination with an abdominal phantom to assess how movement during imaging affected the quality of images and the accuracy of quantitative metrics as shown below in Figure 3.

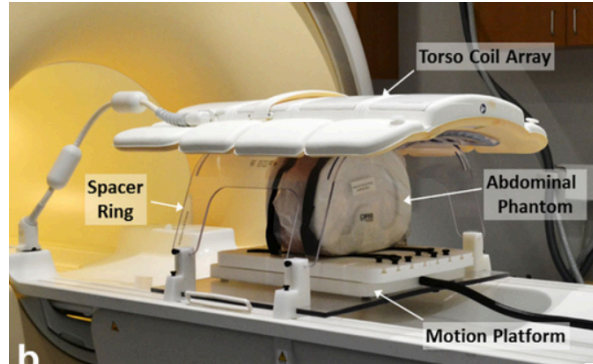


**Figure 3**  
University of Texas Motion Platform [12]

This design consists of a motorized linear stage residing inside the MRI machine and driving electronics outside the MRI room. The motorized stage followed sinusoidal, harmonic, random, or user-defined trajectories. The device was used only for the study and is not on the market for outside use. Additionally this design was very costly, totaling around \$19,000, and was specifically designed for an abdominal phantom [12].

Another competing design is the Vital Biomedical Technologies MRI Compatible Multi-Modality Motion Stage. This device is a programmable linear motion stage as shown below in Figure 4. This product is used in the bore of the MRI scanner and follows user-defined trajectories. The programmed trajectories are loaded onto the control system through a micro SD card.



**Figure 4**  
Vital Biomedical Technologies MRI Compatible Motion Stage [13]

This product has a patent pending and there are a suite of other similar motion stages by this same company to address different anatomical motions [13]. Similar to the previous design this product is limited in phantom compatibility and cannot support the weight of a large phantom. Additionally, this product was also in the five Figure range. Another drawback is that the motor is close to the phantom, which can create signal defects leading to inaccurate or imprecise q-MRI data.

The Quasar MRI Motion Phantom is an MR safe programmable phantom. In this device, the motion capable components are incorporated directly with the phantom as shown below in Figure 5.



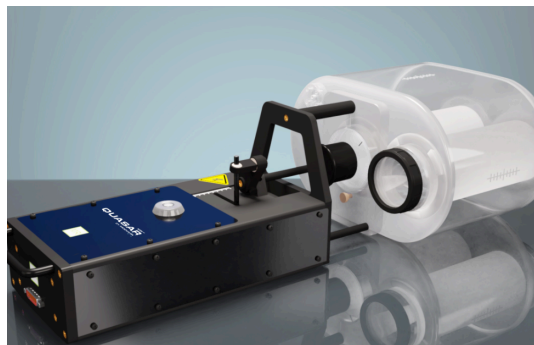


**Figure 5**  
Quasar MRI Motion Phantom [14]

This design uses piezoelectric motors to create desired motions. It is intended to be used to test deep inspiration breath hold protocols. It is unclear how useful this product would be in protocols that require normal respiratory movement rather than breath holding [14]. This was the most expensive of the three competing designs as the client received a quote near \$50,000. In addition to the cost, this design limits what phantoms can be used as it can only hold specific cartridges provided by the company. This design also has motor components close to the phantom, which raises concerns about signal interference similar to the design by Vital Biomedical Technologies.

Each of the current designs on the market come with a number of limitations we hope to overcome. In this study, we report on a sinusoidal motion platform for conducting qMRI testing on abdominal phantoms. The fabrication of the prototype is outlined, along with the tests conducted to evaluate its performance and tolerances.

## Methods

### MRI-Compatible Motion Platform

The MRI motion platform consists of three components. First, a motor assembly that sits at the edge of the MRI bed and drives a drive-shaft that reaches into the MRI bore. Next, a gearbox assembly that converts rotational motion from the motor assembly to linear motion to the phantom bed. Last, control electronics which are held outside of the scan room within the control room.

The motor assembly is driven by a non-magnetic piezoelectric WLG-75-R motor, held in place by a cooling copper face connected to a 3D printed base. The piezoelectric motor generates rotational motion which is transmitted to the gearbox assembly.

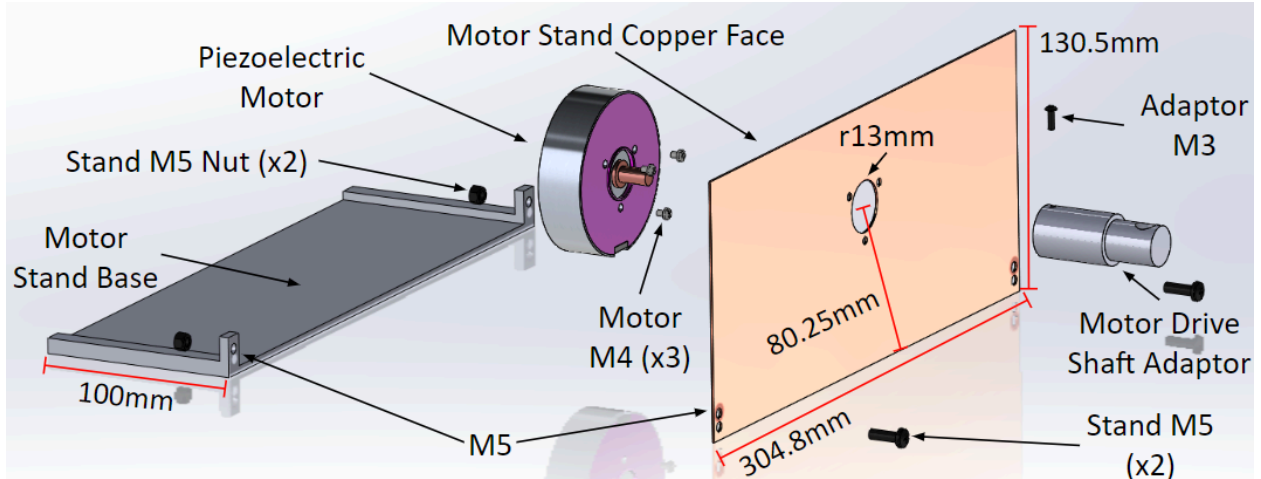


**Figure 6**

Motor Assembly (exploded view). From left to right: Motor Stand Base, WLG-75-R Piezoelectric motor, Motor Stand Copper Face, Motor Drive Shaft Adaptor. The Motor Assembly generates rotational motion which is transmitted down the drive-shaft to the Gearbox Assembly.

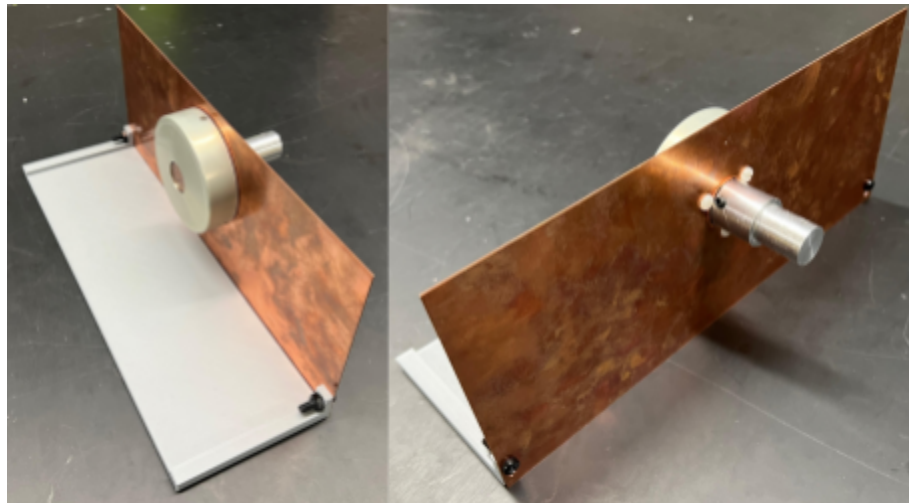


**Figure 7**

Motor Assembly back view (left), Motor Assembly front view (right).

A 4 ft PVC pipe drive-shaft translates rotational motion from the motor assembly to the gearbox assembly. The gearbox assembly shifts the plane of rotation 90 degrees using two bevel gears, and converts the rotational motion to linear motion using a rack and pinion design. The bevel gears are configured to have a 1.5:1 gear ratio to reduce rotation motion from the motor. The linear motion produced is transferred directly to the phantom bed which oscillates on two carbon fiber linear rails.

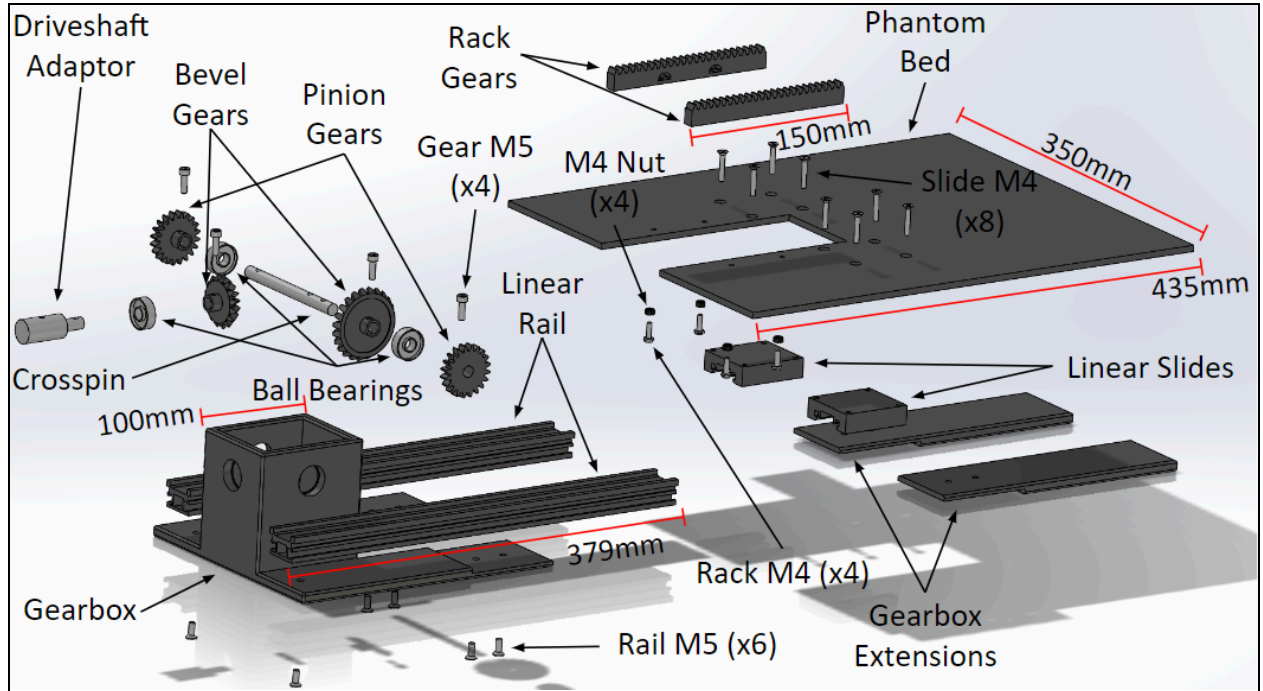


**Figure 8**

Gearbox Assembly (exploded view). From left to right: Gearbox, Gearbox Extensions, Linear Rails, Linear Slides, Phantom Bed, Rack Gears. The Gearbox Assembly takes rotational motion from the Motor Assembly which has been transmitted down the drive-shaft and converts it to linear motion to oscillate the phantom bed.

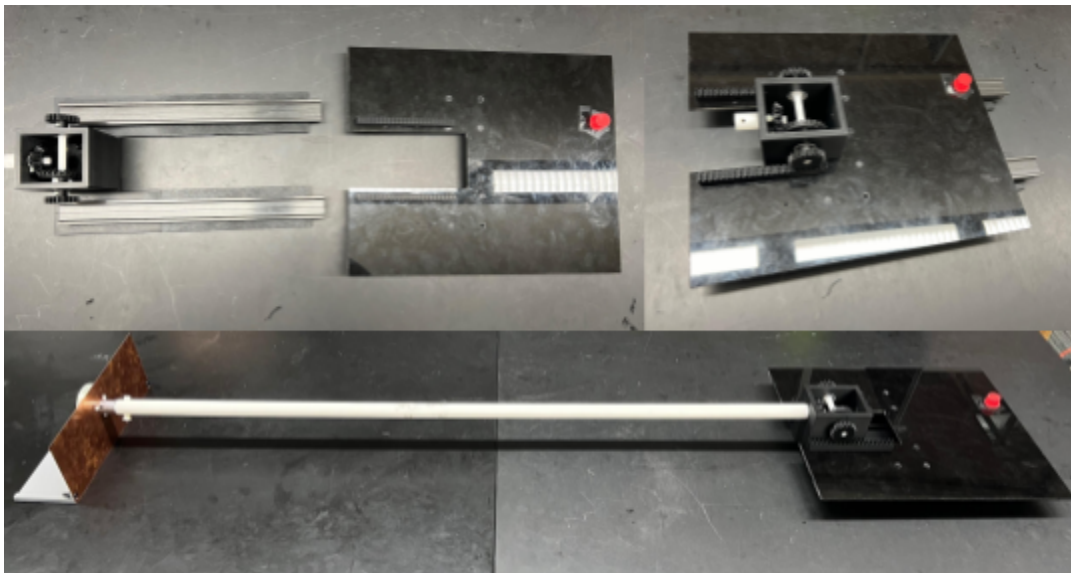


**Figure 9**

Gearbox Assembly with phantom bed removed (top left image), Gearbox Assembly with phantom bed attached (top right image). From left to right: Motor Assembly, PVC drive-shaft, and Gearbox Assembly (bottom image).

The control electronics sit within the control room, and consists of a 96 watt power supply driving a NUCLEO-F446RE microcontroller connected to a motor control board. The motor control board connects to the motor assembly via a braided wire that fits through a small entry port from the control room to the scan room.

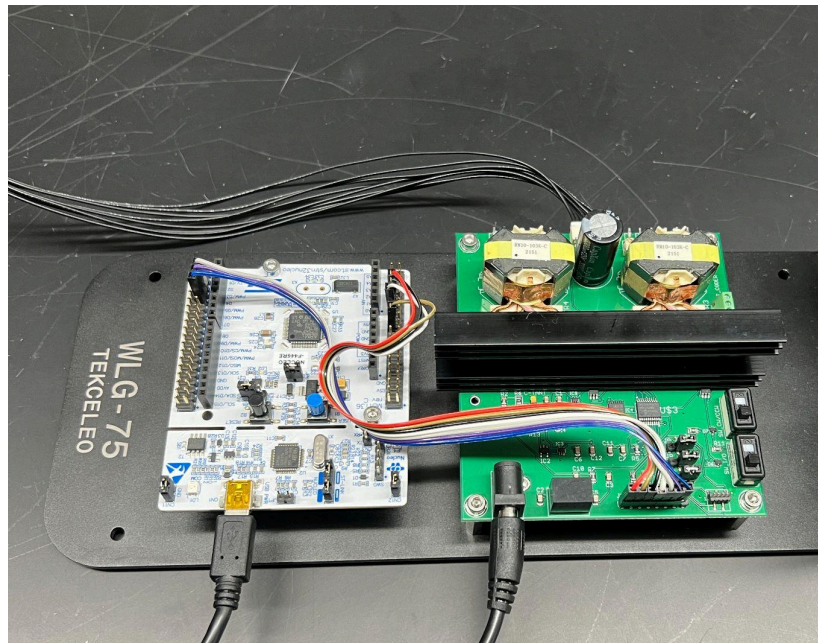


**Figure 10**

Illustrates the control electronics which will be contained within the MRI control room. The board on the left is the NUCLEO-F446RE microcontroller which controls the green board on the right which is the motor control board. The control electronics control the Motor Assembly via a braided cable which connects via a port hole into the scan room.

## Characterization of Motion

Studies have been performed to track the movement of internal organs due to respirations using external signals [15]. Based on this data, liver movement due to respiration has been shown to be sinusoidal at a frequency of 8 cycles per minute and an amplitude of 3 cm [15]. Using the data of a typical sinusoidal respiratory motion, the required motor torque was calculated. The torque was calculated by taking the second derivative of the position equation. The position equation is  $3 \text{ cm} \times \sin(2\pi \times (8/60) \times t)$ . Taking the derivative with respect to time, the velocity is calculated to be  $3 \text{ cm} \times (\pi \times 8/30) \times \cos(\pi \times (8/30) \times t)$ . Taking the second derivative with respect to time, the acceleration is calculated to be  $3 \text{ cm} \times (\pi \times 8/30)^2 \times \sin(\pi \times (8/30) \times t)$ . From this equation, the maximum acceleration is determined to be  $2.1 \text{ cm/s}^2$ . The maximum acceleration, radius of the pinion, and estimated mass of 4 kg can be applied to the fundamental equation of torque,  $\tau = rma$ , to find the required maximum torque. The required torque is calculated by  $21.64 \text{ cm} \times 4 \text{ kg} \times 2.1 \text{ cm/s}^2$  and found to be  $1.82 \times 10^{-3} \text{ Nm}$ . The motor

specifications list a maximum torque of 1.2 Nm; therefore, the motor is within the limits of the assembly [16].

## Sinusoidal Motion Test

The sinusoidal motion test was performed to determine if the platform would move at the expected displacement of the sine wave. We performed 3 rounds of testing. In the first round of testing trials were conducted at different weights, but the motor velocity remained constant throughout trials. The prototype was assessed on how accurate the displacement was over the course of the test in comparison to expected displacement. The expected displacement was calculated by taking the integral of the motor velocity with respect to time. Motor Velocity =  $A \times \sin(2\pi \times f \times t)$ , therefore, Expected Displacement =  $A / (2\pi \times f \times t) \times \cos(2\pi \times f \times t)$ . This was key in determining if the accuracy of the sinusoidal motion remained within 5% deviation.

To perform this test, a bright marker was placed on the platform to mark the initial position. Then a recording was taken from above for a full view of the platform. We began running "sinusoidalSpeedVariation()" on Mbed by pressing 2. This program sets the velocity of the motor to a sine wave that varies over time for 60 seconds. At the end of the trial we stopped the recording. Displacement was measured throughout the entire time the motor is moving using Kinovea. Key aspects of the wave were then identified and compared to the expected wave to determine the accuracy of the sinusoidal motion.

After making modifications to the prototype and software after preliminary testing, another round of testing was performed. In this secondary round of testing trials were conducted at various weights, amplitudes, and frequencies. The secondary round of weight trials were conducted at various weights ranging from 0 kg - 4 kg. Based on the results the motor was recalibrated and then a third round of weight testing was performed. A final round of testing assessed the bounds of the prototype's amplitudes and frequencies. Three trials were performed for each amplitude and frequency variation. The amplitudes tested included 1 cm and 6 cm at a frequency of 8 cycles per minute to compare to the baseline 0 kg test. Frequencies tested included both 4 cycles per minute and 20 cycles per minute at an amplitude of 3.6 cm to compare to the baseline 0 kg test.

## MR-Compatibility Test

To ensure the device was safe to use in the MR environment, the prototype was inspected by a certified Medical Radiologist using a strong hand magnet. The prototype was tested in the bore of the MRI as it would be used by researchers. While in the MRI machine the device was assessed for overall functioning and interference with image quality.

## Future Work

Prospective tests include extended motion tests and revision of amplitude and frequency tests. The extended motion test would be formatted similar to the sinusoidal motion test, but

would run for 15 minutes instead of 1 minute. This would be necessary to satisfy the PDS runtime requirement. The results would determine the extended accuracy and reliability of the sinusoidal motion over a more realistic acquisition time frame.

The amplitude and frequency test would be recollected due to potential error in image distortion and Kinovea calculations in previous tests. The recollection of data from this test would help represent more accurate data in regard to the prototype's ability to meet specifications at extreme amplitudes and frequencies.

## Results & Discussion

### MRI-Compatible Motion Platform

A Tekceleo WLG-75-R Motor piezoelectric motor is utilized in the motor assembly. The WLG-75-R motor has a maximum output of 150 RPM with a 1.2 Nm load. The motor's maximum outputs determine the maximum outputs of the gearbox. The following equations determine the required RPM and induced torque on the motor with a phantom mass (kg) input and desired outputs amplitude (cm), and frequency (cycles/minute).

$$RPM = \frac{\left(\frac{2*\pi*frequency*amplitude}{6000}\right)}{\left(\frac{0.044*\pi}{60*gear\_ratio}\right)}$$

**Equation 1.** Required RPM

$$Torque = \frac{gear\_ratio*mass*0.044*2*\pi^2*frequency^2*amplitude}{360000}$$

**Equation 2.** Induced Torque

When utilizing a 1:1 gear-ratio within the gearbox for a 10 kg phantom, maximum outputs are limited to 55 cycles/minute at an amplitude of 6 cm, or 60 cycles/min at an amplitude of 5.5 cm. For improved performance, a 1.5:1 gear-ratio may be used, which limits the gearbox outputs to 36 cycles/sec at an amplitude of 6 cm, or 60 cycles/sec at an amplitude of 3.67 cm.



### Gear-Ratio 1:1

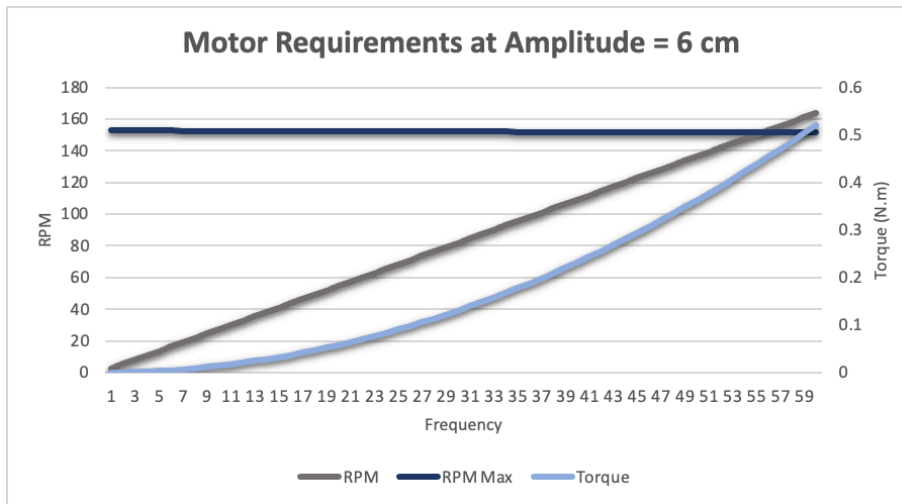


**Figure 11**  
 Motor limitations graph with a 10 kg phantom while configured to have a 1:1 gear ratio. Motor RPM requirement at 6 cm amplitude with varying frequency (gray), Motor torque at 6 cm amplitude with varying frequency (light blue), and maximum possible motor RPM output (dark blue).

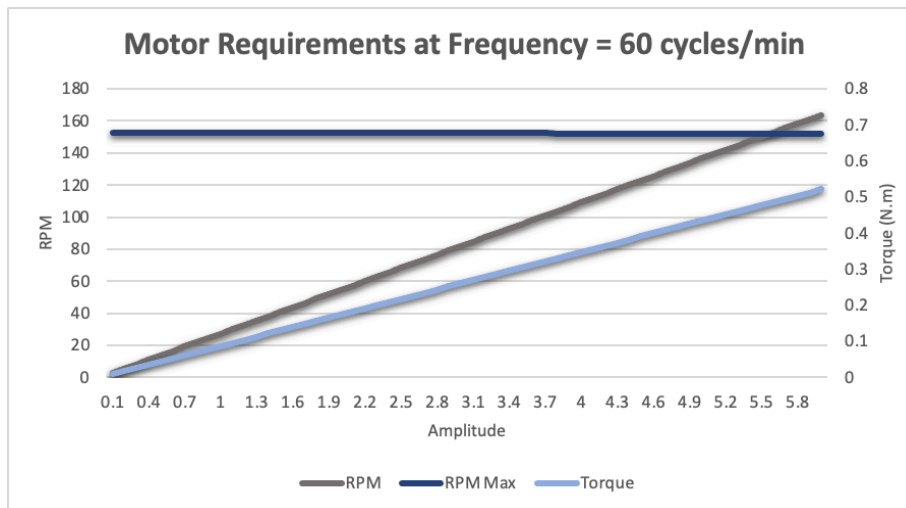


**Figure 12**  
 Motor limitations graph with a 10 kg phantom while configured to have a 1:1 gear ratio. Motor RPM requirement at 60 cycles/min with varying amplitude (gray), Motor torque at 60 cycles/min with varying amplitude (light blue), and maximum possible motor RPM output (dark blue).



### Gear-Ratio 1.5:1

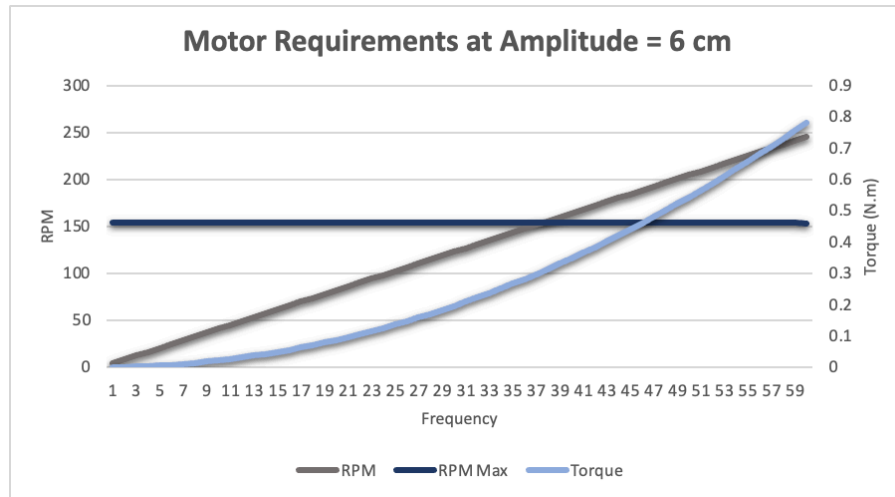


**Figure 13**

Motor limitations graph with a 10 kg phantom while configured to have a 1.5:1 gear ratio. Motor RPM requirement at 6 cm amplitude with varying frequency (gray), Motor torque at 6 cm amplitude with varying frequency (light blue), and maximum possible motor RPM output (dark blue).

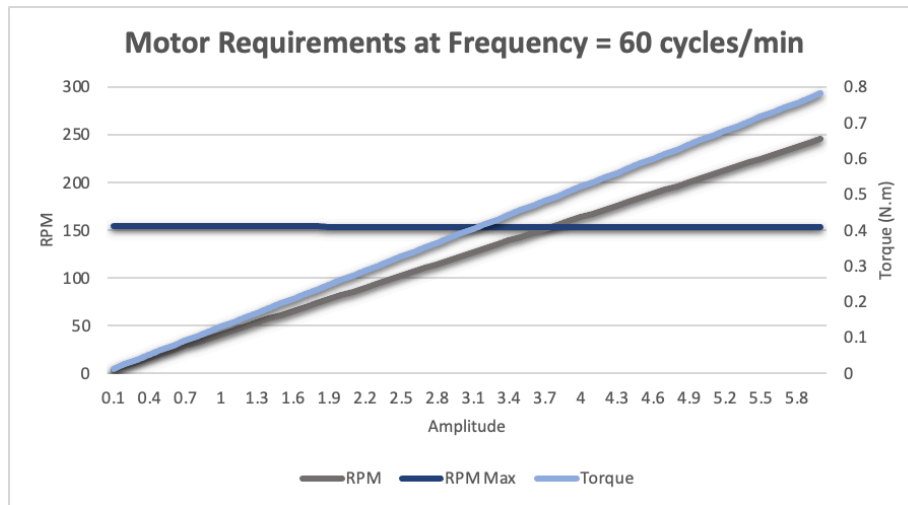


**Figure 14**

Motor limitations graph with a 10 kg phantom while configured to have a 1.5:1 gear ratio. Motor RPM requirement at 60 cycles/min with varying amplitude (gray), Motor torque at 60 cycles/min with varying amplitude (light blue), and maximum possible motor RPM output (dark blue).

## Characterization of Motion

As discussed in the methods section, the motion of the platform must be sinusoidal. In order to accomplish this, a NUCLEO-F446RE microcontroller was programmed to control the motor velocity through a motor control board. Key features of the setup include the motor encoder object. This object has properties to read the state of the encoder, read the number of pulses recorded by the encoder, and read the number of revolutions recorded by the encoder on the index channel [17]. Additionally, 3 pins were configured to direct the motors velocity, direction, and state (ON/OFF).

The sinusoidalSpeedVariation function was programmed to vary the motor speed sinusoidally. The sine wave produced by the code has a set amplitude and frequency. Depending on the sign of the wave, the motor will either move clockwise or counterclockwise. In order to produce a wave of consistent frequency throughout the function, an Interrupt Service Routine (ISR) is called every  $1/(360 \times f) \times 10^6$  microseconds. Each period of the sine wave is plotted with 360 points, giving an analog output value for every  $1^\circ$  of the sine wave. After the sine function is calculated, the desired RPM is converted to a hex velocity using a voltage conversion factor. The voltage conversion factor was calculated based on the Tekceleo getting started guide, and is currently equal to  $1/175$  [16].

## Sinusoidal Motion Test

### Preliminary Weight Test

The sinusoidal motion test was performed with 0 kg of added weight and 4 kg of added weight. Plots of displacement over time were created for each trial. The expected displacement curve can be seen in orange, while the experimental displacement curve can be seen in blue.

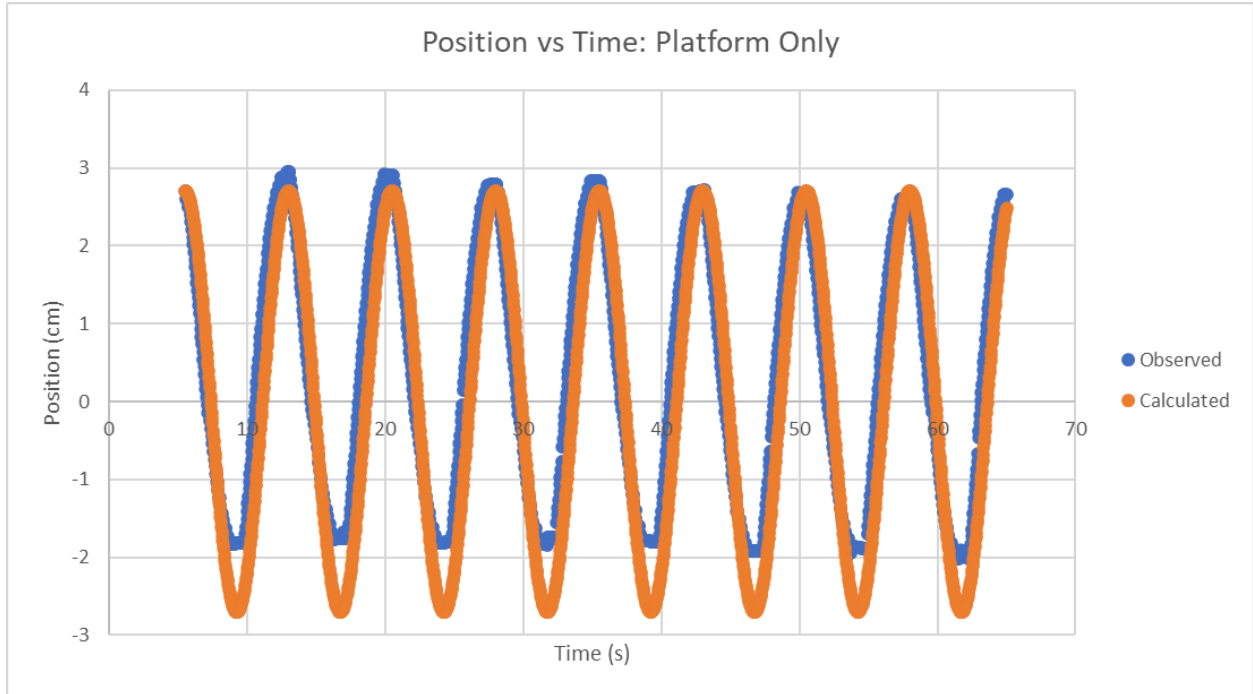


**Figure 15**

Position vs. Time graph with weight of the platform only.

The time between peaks was measured to be  $7.50 \pm 0.4$  s with a 3.87% error. The expected value is 7.50 seconds, as determined by the set frequency of 8/60 cycles/s. The peak to peak amplitude was measured to be  $4.619 \pm 0.07$  cm with a 14.63% error. The expected value is 5.41 cm, which is double the input of 10 RPM, which is equal to 2.705 cm/s. In this trial, the time between peaks is within the 5% tolerance set by the PDS, but the peak to peak amplitude is not.

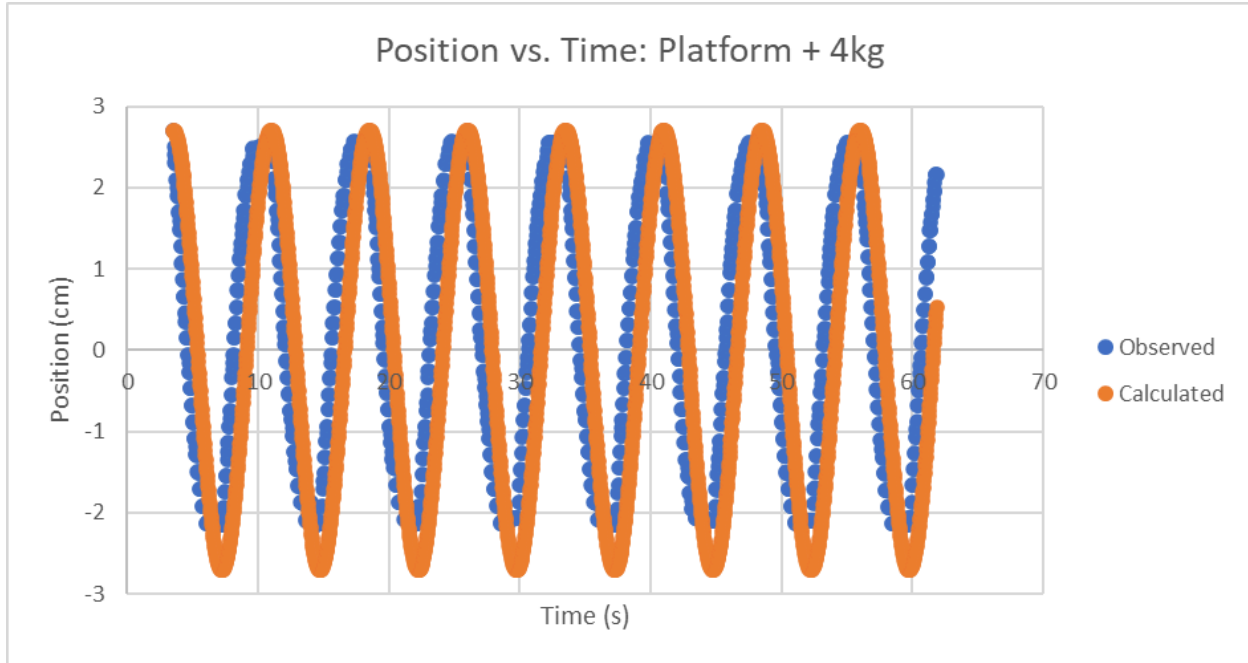


**Figure 16**

Position vs. Time graph with weight of the platform plus 4 kg.

The time between peaks was measured to be  $7.50 \pm 0.7$  seconds with a 7.30% error. The expected value is 7.50 seconds, as determined by the set frequency of 8/60 cycles/s. The peak to peak amplitude was measured to be  $4.685 \pm 0.05$  cm with a 13.39% error. The expected value is 5.41 cm, which is double the input of 10 RPM, which is equal to 2.705 cm/s. In this trial, the time between peaks and the peak to peak amplitude is not within the 5% tolerance set by the PDS.

Both sinusoidal motion tests showed that the observed displacement wave led the calculated displacement wave in both trials. The displacement graphs exhibited sinusoidal motion similar to what was expected. When looking at the expected end point of the experiment, there was variation between the observed and calculated final positions. With increased weight, this difference was more prominent. The time between peaks was on average the most accurate, but at the desired 4 kg weight it did not meet the 5% specification outlined in the PDS. Both trials of peak to peak amplitude were outside of the PDS accuracy specification.

## Secondary Weight Test

The sinusoidal motion test was performed with 0 kg, 1.5 kg, and 3.56 kg of added weight. Three trials were performed for each weight test. Only one trial is plotted in Figure 17. The experimental displacement curve can be seen in red for 0 kg, blue for 1.5 kg, and green for 3.56 kg.

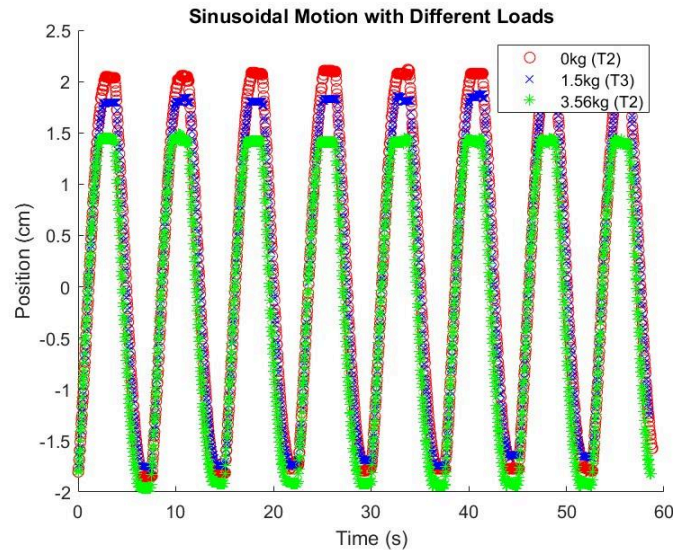


**Figure 17**  
Position vs. Time graph of secondary weight test.

For 0 kg, the time between peaks was measured to be  $7.47 \pm 0.5$  s with a 0.44% error. For 1.5 kg, the time between peaks was measured to be  $7.60 \pm 0.6$  s with a 1.38% error. For 3.56 kg, the time between peaks was measured to be  $7.55 \pm 0.5$  s with a 0.71% error. The expected value is 7.50 seconds, as determined by the set frequency of 8/60 cycles/s. At all 3 weights, the period was within the 5% tolerance set by the PDS.

For 0 kg, the peak to peak amplitude was measured to be  $3.79 \pm 0.08$  cm with a 3.48% error. For 1.5 kg, the peak to peak amplitude was measured to be  $3.57 \pm 0.06$  cm with a 2.51% error. For 3.56 kg, the peak to peak amplitude was measured to be  $3.41 \pm 0.2$  cm with a 7.03% error. The expected value is 3.67 cm. The 0 kg and 1.5 kg peak to peak amplitudes were within the 5% tolerance set by the PDS, but the 3.56 peak to peak amplitude was not.

## Recalibrated Weight Test

Once the RPM to voltage coefficient was calibrated, the sinusoidal motion test was performed with 0 kg and 1.5 kg of added weight. Three trials were performed for each weight test. Only one trial is plotted in Figure 18. The experimental displacement curve can be seen in red for 0 kg and blue for 1.5 kg.

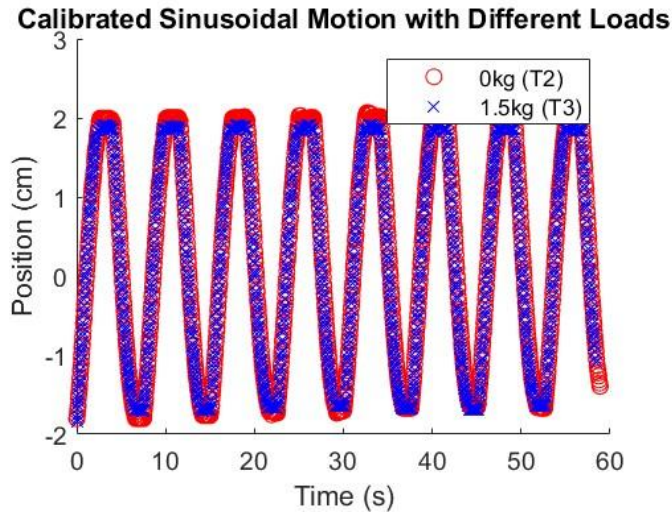


**Figure 18**  
Position vs. Time graph of calibrated weight test.

For 0 kg, the time between peaks was measured to be  $7.50 \pm 0.6$  s with a 0.06% error. For 1.5 kg, the time between peaks was measured to be  $7.50 \pm 0.4$  s with a 0.02% error. The expected value is 7.50 seconds, as determined by the set frequency of 8/60 cycles/s. At both weights, the period was within the 5% tolerance set by the PDS and improved when compared to the uncalibrated trial.

For 0 kg, the peak to peak amplitude was measured to be  $3.78 \pm 0.05$  cm with a 3.12% error. For 1.5 kg, the peak to peak amplitude was measured to be  $3.67 \pm 0.2$  cm with a 0.10% error. The expected value is 3.67 cm. The 0 kg and 1.5 kg peak to peak amplitudes were within the 5% tolerance set by the PDS and improved when compared to the uncalibrated trial.

## Frequency and Amplitude Bound Test

Three trials were performed for each frequency. Only one trial for each is plotted below in Figure 19. The low frequency bound was 4 cycles per minute and is shown below in red. The high frequency bound was 20 cycles per minute and is shown below in blue.

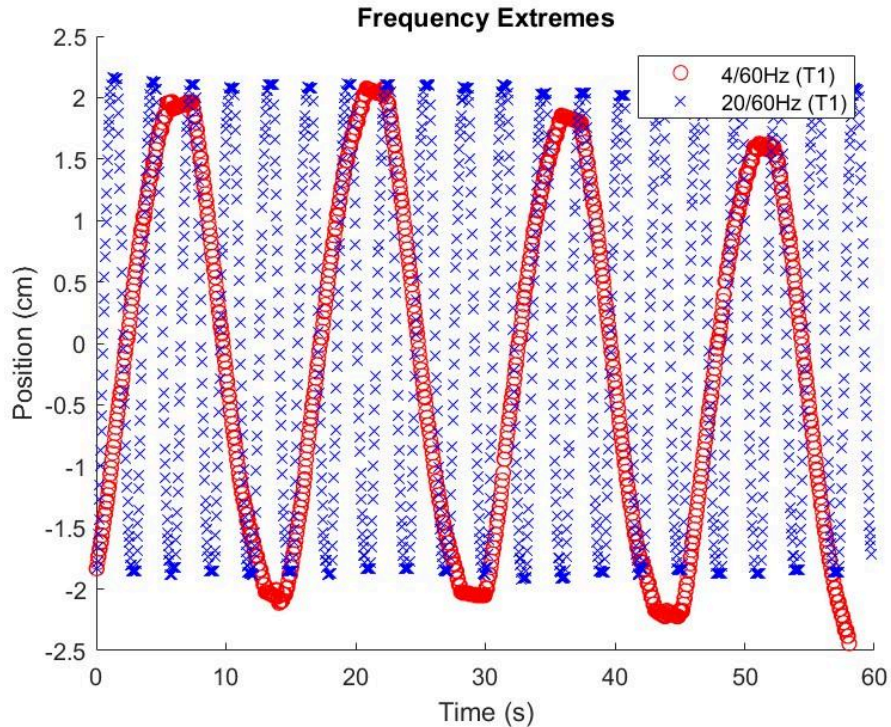


**Figure 19**  
Position vs. Time graph for Frequency Extremes.

The time between peaks for the low frequency was measured to be  $15.1 \pm 0.7$  s with a 0.45% error. The expected value is 15 seconds as determined by the set frequency of 4/60 cycles/s. This is well within the 5% tolerance set by the PDS. The time between peaks for the high frequency was measured to be  $3.02 \pm 0.2$  s with a 0.51% error. The expected value is 3 seconds as determined by the set frequency of 20/60 cycles/s. This is also well within the 5% tolerance set by the PDS.

Three trials were also performed for each amplitude. Only one trial for each is plotted below in Figure 20. The low amplitude bound was 1 cm and is shown below in green. The high amplitude was 6 cm and is shown below in pink. During the 1 cm trial there was significant play between the gears and a disconnect between the driveshaft and the motor. Because of this only 1 valid trial for the 1 cm test was obtained. Due to limited time in the semester, retesting was not able to be performed.



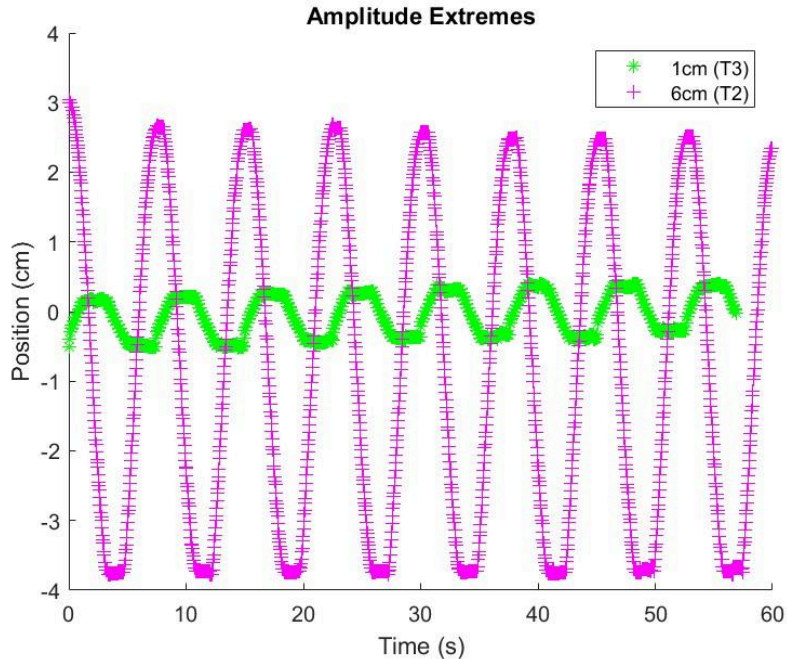


**Figure 20**  
Position vs. Time for Amplitude Extremes.

The peak to peak amplitude for the lower bound was measured to be  $0.736 \pm 0.04$  cm with a 27.63% error. The expected value is 1.02 cm. This was not within the 5% tolerance outlined in the PDS. The peak to peak amplitude for the upper bound was measured to be  $6.48 \pm 0.2$  cm with a 6.16% error. The expected value is 6.10 cm. This was not within the 5% tolerance outlined in the PDS.

## MR-Compatibility Test

The prototype passed the initial inspection with the hand magnet and was then brought into the MRI room piece by piece. The prototype functioned normally both outside and inside the bore while in the MRI room. Initial imaging revealed RF noise brought into the MRI room via the cable for the motor. More testing should be done to minimize this noise. Likely a low-pass filter could be added to the circuit before the connection to the motor to reduce this noise. Additionally, covering the cable through the hole into the MRI room with aluminum may help to minimize the noise.

## Future Work

The testing results can be summarized as follows. Over all tests, there was low period error and acceptable amplitude error. During the weight tests, there was no observable relationship with weight. Furthermore, calibration improved percent error in period and amplitude. Finally, the amplitude extremes were not within tolerance.

Some sources of error can be attributed to these results. First, the motor code producing the sine wave operated the motor driver with a small input range (voltage input from code was ~0.2 V when the maximum input was 3.3 V). Next, the Kinovea tracking software and testing setup was imperfect. Through experimentation it was found that even small errors in the angle of the camera, FOV of the camera, and tracking of the marker led to extreme discrepancies in the data. There was also an imperfect RPM to Voltage conversion as it had to be calibrated experimentally. Finally, play between gears and driveshaft dislodgement could have amounted to error in the amplitude.

Changes to the design that will improve the prototype's ability to meet design specifications include implement proportional control, optimize gear interactions, add additional sliders, include flexible coupling, and reposition ball bearings. The motor includes a built in encoder that can be used to produce a proportional control system based on positioning feedback. This proportional control will help reduce the positioning error of the motor output. The gear interactions inside the gearbox and between the rack and pinion could be optimized by increasing the gear tooth fillet fit. Additional sliders could be used to reduce the torque required from the motor and help move the phantoms with ease. The motor specifications suggest including a flexible coupling between the motor and the drive shaft to prevent axial loading [16]. If the insertion points of the ball bearings were flipped to be within the gearbox, the results would likely show less gear slippage and more accuracy.

After design changes are made based on current and prospective testing results, the prototype can be developed further in a few directions. The first direction is the inclusion of the low-pass filter that will reduce radio frequency noise between the control room and the MRI room. Another direction is to develop the user interface to be able to fluctuate the amplitude and frequency of the sinusoidal waveform with ease. Lastly, the design could be retrofitted to replicate high frequency cardiac motion, along with other physiological motions.

## Conclusions

Currently, products designed for qMRI research are limited to specific phantoms and are extremely expensive. This new, open-source motion platform would improve diagnostic capabilities for patients unable to perform current image artifact mitigation procedures. This design features a 3D printed gearbox which converts rotational motion from the ultrasonic motor to the phantom bed via a rack and pinion mechanism. The racks are screwed onto an acrylic platform, which sits on linear slides to reduce friction. The motor is programmed to produce a sinusoidal wave to mimic anatomical breathing.

Preliminary testing included motor RPM validation and optical tracking of the platform when loaded with different masses. Movement data was tracked and analyzed using Kinovea. The experimental sine wave was compared to the wave input into the motor. A comparison of peak to peak times as well as amplitudes proved that experimental motion did not properly track with the input wave. RPM testing revealed that the input motor RPM was significantly higher than what was being output by the motor. This was likely a key factor in the movement discrepancy found previously.

After preliminary testing modifications were made to both the mechanical and software aspects of the design. In terms of mechanical changes, the gearbox was redesigned to be able

to support a 1:1, 1.5:1, and 2:1 gear ratio. The prototype was rebuilt with the 1.5:1 gear ratio for additional testing. In terms of the software, an interrupt service routine was added to the code to allow for more precise control of the motor. Testing was then performed to assess the performance of the updated prototype. The sinusoidal motion test was performed again and revealed that the amplitude was still not always within the specified tolerance. In order to address this, the motor was experimentally recalibrated. The major source of error causing the difference in amplitude was the RPM to voltage conversion factor in the code. The original conversion coefficient was within the provided motor source code; however, after extensive testing this coefficient was found to be inaccurate. Through experimental trials, the coefficient was improved and further sinusoidal motion testing was conducted. After recalibration, both the period and amplitude were consistently within the specified tolerance.

The sinusoidal motion test was then performed again with modified frequencies and amplitudes in order to test the extreme bounds. This testing revealed that both frequency bounds are within tolerance. However, the amplitude extremes were not within the specified 5% tolerance. Future modifications to the mechanical design may include optimizing gear interactions, flipping the ball bearing insertions, and adding additional sliders to reduce friction. On the software side, implementing proportional control for position feedback using a built-in encoder, as well as utilizing a larger range of the available motor input range for the motor driver, may help increase the accuracy of the amplitude.

As this device is developed and ultimately used in the field, it is important to discuss ethical considerations. During development, it is important to maintain transparency with the client and research group who is funding the project. This includes sharing accurate information about project progress, setbacks, and limitations. This will establish clear accountability for the development and use of the technology. An additional consideration during development is that the final prototype is accessible and affordable. The design is meant to be affordable and accessible to a wide range of researchers, especially those who cannot afford current solutions. This is in-line with the current focus of the device to be open access. This helps promote advancement in medical research without barriers of intellectual property protection. Finally, safety and reliability should be prioritized to avoid harm to users of the technology. This can be ensured through future testing and validation of the device. It is important to continuously monitor and improve the technology to address any emerging ethical concerns or issues.

Overall this device has the potential to act as an important research tool in validating and testing qMRI protocols. This will improve the diagnostic capabilities of healthcare professionals and allow for better patient outcomes.

## Acknowledgements

The team would like to thank our advisor, Dr. James Trevathan, and our client, Mr. Jiayi Tang, for their support and guidance. Additional thanks to Dr. Samuel Hurley, Dr. Amit Nimunkar, and the rest of the UW-Madison BME design staff for their help in the design process.

# References

- [1] "Broadening the Use of Quantitative MRI, a New Approach to Diagnostics." Accessed: Feb. 27, 2024. [Online]. Available: <https://hai.stanford.edu/news/broadening-use-quantitative-mri-new-approach-diagnostics>
- [2] A. Seiler *et al.*, "Multiparametric Quantitative MRI in Neurological Diseases," *Front. Neurol.*, vol. 12, 2021, Accessed: Feb. 27, 2024. [Online]. Available: <https://www.frontiersin.org/journals/neurology/articles/10.3389/fneur.2021.640239>
- [3] K. E. Keenan *et al.*, "Recommendations Towards Standards for Quantitative MRI (qMRI) and Outstanding Needs," *J. Magn. Reson. Imaging JMRI*, vol. 49, no. 7, pp. e26–e39, Jun. 2019, doi: 10.1002/jmri.26598.
- [4] S. van Hees, J. P. D. Kleinloog, A. Sbrizzi, and W. P. C. Boon, "Static Future Technologies, Dynamic Professionalism — Co-creating Future Scenarios in Medical Imaging Practices," *Postdigital Sci. Educ.*, vol. 6, no. 1, pp. 135–153, Mar. 2024, doi: 10.1007/s42438-023-00444-2.
- [5] D. A. Feinberg, N. M. Rofsky, and G. Johnson, "Multiple breath-hold averaging (MBA) method for increased SNR in abdominal MRI," *Magn. Reson. Med.*, vol. 34, no. 6, pp. 905–909, Dec. 1995, doi: 10.1002/mrm.1910340617.
- [6] M. Kocaoglu, A. S. Pednekar, H. Wang, T. Alsaied, M. D. Taylor, and M. S. Rattan, "Breath-hold and free-breathing quantitative assessment of biventricular volume and function using compressed SENSE: a clinical validation in children and young adults," *J. Cardiovasc. Magn. Reson.*, vol. 22, no. 1, p. 54, Jul. 2020, doi: 10.1186/s12968-020-00642-y.
- [7] "About," CaliberMRI. Accessed: Feb. 27, 2024. [Online]. Available: <https://qmri.com/about/>
- [8] J. Nofiele *et al.*, "An MRI-compatible platform for one-dimensional motion management studies in MRI," *Magn. Reson. Med.*, vol. 76, no. 2, pp. 702–712, Aug. 2016, doi: 10.1002/mrm.25903.
- [9] P. Bannas *et al.*, "Quantitative magnetic resonance imaging of hepatic steatosis: Validation in ex vivo human livers," *Hepatol. Baltim. Md*, vol. 62, no. 5, pp. 1444–1455, Nov. 2015, doi: 10.1002/hep.28012.
- [10] "Nonalcoholic fatty liver disease - Symptoms and causes - Mayo Clinic." Accessed: Feb. 27, 2024. [Online]. Available: <https://www.mayoclinic.org/diseases-conditions/nonalcoholic-fatty-liver-disease/symptoms-causes/syc-20354567>
- [11] C. Arboleda *et al.*, "Total liver fat quantification using three-dimensional respiratory self-navigated MRI sequence," *Magn. Reson. Med.*, vol. 76, no. 5, pp. 1400–1409, Nov. 2016, doi: 10.1002/mrm.26028.
- [12] W. T. Reichert, "A Simple Multi-Parametric Quantitative MRI Phantom".
- [13] "Motion Stages Compatible with CT, MRI, PET, SPECT & Ultrasound." Accessed: Feb. 27, 2024. [Online]. Available: <https://www.simutec.com/Products/motionstages.html>
- [14] "QUASAR™ MRI<sup>4D</sup> Motion Phantom," Modus Medical Devices. Accessed: Feb. 27, 2024. [Online]. Available: <https://modusqa.com/products/quasar-mri4d-motion-phantom/>
- [15] S. Fahmi, F. F. J. Simonis, and M. Abayazid, "Respiratory motion estimation of the liver with abdominal motion as a surrogate," *Int. J. Med. Robot.*, vol. 14, no. 6, p. e1940, Dec. 2018, doi: 10.1002/rcs.1940.
- [16] "Our Resources - Tekceleo," <https://www.tekceleo.com/>. Accessed: Feb. 25, 2024. [Online]. Available: <https://www.tekceleo.com/our-resources/>
- [17] "QEI - Cookbook | Mbed." Accessed: Feb. 25, 2024. [Online]. Available: <https://os.mbed.com/cookbook/QEI>

# Appendix

## A. PDS

### **MRI Compatible Motion Platform - BME 400**

*Product Design Specifications*

February 27th, 2024

**Client:** Mr. Jiayi Tang

**Advisor:** Dr. James Trevathan

**Team:** Maxwell Naslund - Team Leader  
Kendra Besser - Communicator  
Amber Schneider - BWIG  
Jamie Flogel - BPAG  
Caspar Uy - BSAC

#### **Function**

MRI phantoms are often static models of the human body that are used to test and calibrate MRI's. Natural process' such as respiration and digestion create constant motion within the human body. Static phantoms used to calibrate MRI's do not properly represent this motion. This demonstrates a need for an MR compatible device that holds a phantom and is capable of simulating the movements found within the human body.

#### **Client requirements:**

- MR Compatible
- Moves back and forth
- Minimize the use of electronics inside the room
- Potentially incorporate materials currently available from the client
- Create a prototype with a budget of \$1000
- Utilize commercially available parts
- Avoid complex fabrication methods

#### **Design requirements:**

## 1. Physical and Operational Characteristics

- a. *Performance requirements:* The product will be a magnetic resonance compatible platform that provides a periodic waveform motion. The waveform motion will have a frequency of 4-20 cycles/min and amplitude of 1-6 cm to represent physiological breathing patterns. The motion will be consistent for 15 minutes and is allotted a standard deviation of 5% from the desired waveform. The product must withstand the size and weight of a phantom liver for testing purposes.
- b. *Safety:* The device will be entirely made of MR compatible material and will pose no safety risk within the MR environment. The device's magnetically induced displacement and torque forces will be tested to assure these forces are below their gravitational equivalents. The device will also be evaluated for RF heating, eddy currents, gradient induced vibrations, and gradient induced extrinsic electrical potential risks, as also recommended by the FDA [1]. As this device will utilize electronics, it is classified as an active medical device and will follow FDA 21 CFR part 801 and ASTM F2503 labeling requirements.
- c. *Accuracy and Reliability:* The device must be able to produce repeatable patterns of movements within 2mm. The components of the device must not decrease the signal to noise ratio of the calibration phantom being tested. The device must be able to reliably repeat MR scans with minimal decrease in image quality between scans.
- d. *Life in Service:* The device must operate for up to 60 minutes at a time as that is the time an MRI may take to produce an image of a medium-sized area [2]. A non-magnetic motor should last 20,000 hours under normal operating conditions [3]. Overall the device should last as long as an MRI scanner, which is approximately 10 years [4].
- e. *Shelf Life:* Based on the motor components it should be stored in -40 to 70 °C temperatures with humidity 0 to 80% non condensing [2].
- f. *Operating Environment:* The device must be able to withstand upwards of 3 tesla for 1 hour [5]. The device must be able to withstand potential RF heating, eddy currents, gradient induced vibrations, and gradient induced extrinsic electrical potential risks associated with devices within strong magnetic fields [1].
- g. *Ergonomics:* The platform should have a height that is comfortable and safe for people to interact with when placed in the MRI. No force should be applied by a person to the motor or any moving parts during operation. An emergency stop feature should be implemented to allow users to immediately stop the motion platform in case of any issues or safety concerns.
- h. *Size:* The platform will be no smaller than 25cm x 35cm in order to hold a

range of phantom liver samples [6]. The platform will be rectangular shaped.

i. *Weight*: In order for the user to install and uninstall the platform during each segment of testing, the weight should not exceed 10kg. The platform must be able to withstand 4kg [7].

j. *Materials*: The product will be composed of MRI compatible materials. Ferrous and magnetic metals will not be used; other metals, such as brass and aluminum, will be limited to minimize the possibility of induced currents. A nonmagnetic ultrasonic piezoelectric motor will be used to provide platform motion. Nonmetallic sliding rails and bearings will be used to guide the platform through the MRI machine.

k. *Aesthetics, Appearance, and Finish*: Color, shape, form, texture of finish should be specified where possible (get opinions from as many sources as possible).

## **2. Production Characteristics**

a. *Quantity*: Produce one motion controlled platform.

b. *Target Product Cost*: The budget for this project is \$1000 with many of the components already provided including some motors, rails, software, and hardware. Existing MRI compatible designs cost around \$9700 excluding the cost of the phantom used [7].

## **3. Miscellaneous**

a. *Standards and Specifications*: MRI systems and accessories must follow the multiple sets of standards designed by the organizations like the FDA involving forms of testing the functionality of the machine including any additional accessories. Accessory parts should allow appropriate function in testing MRI displacement force ASTM F2052, torque ASTM F2213, RF heating ASTM F2182, and image artifact ASTM F2119 [8].

b. *Customer*: Preferences on stability and levelness will assist users in creating more genuine images. Reducing additional noise from both the platform and machine would be beneficial to more optimal usage.

c. *Patient-related concerns*: The device would need to be appropriately cleaned and disinfected for each use as instructed with the associated manufacturer. Appropriate dimensions levelness of the platform will need to be monitored to help with specimen/subject safety. Additionally cleanliness of the machine is an important consideration as the device should not leak motor oil or other fluids on the MRI bed.



*d. Competition:*

- Vital Biomedical Technologies MRI Compatible Multi-Modality Motion Stage is a programmable linear motion stage. This product is used in the bore of the MRI scanner and follows user-defined trajectories. The programmed trajectories are loaded onto the control system through a micro SD card. This product has a patent pending and there are a suite of other similar motion stages by this same company to address different anatomical motions [9].
- For a study done by the Department of Radiology at University of Texas Southwestern Medical Center researchers developed a one-dimensional MRI compatible motion platform. They used this in combination with an abdominal phantom to assess how movement during imaging affected the quality of images and the accuracy of quantitative metrics. This design consisted of a motorized linear stage residing inside the MRI machine and driving electronics outside the MRI room. The motorized stage followed sinusoidal, harmonic, random or user-defined trajectories. The device was used for the study and is not on the market for outside use [7].
- The Quasar MRI Motion Phantom is a completely MR safe programmable phantom. In this device the motion capable components are incorporated directly with the phantom. This design uses piezoelectric motors to create desired motions. It is intended to be used to test Deep Inspiration Breath Hold protocols. It is unclear how useful this product would be in protocols that require normal respiratory movement rather than breath holding [10].

## References

- [1] "Testing and labeling medical devices for safety in the magnetic ...," U.S. FOOD & DRUG ADMINISTRATION, <https://www.fda.gov/media/74201/download?attachment> (accessed Sep. 22, 2023).
- [2] "How it's performed - MRI Scan," NHS choices, [https://www.nhs.uk/conditions/mri-scan/what-happens/#:~:text=A%20magnetic%20resonance%20imaging%20\(MRI,number%20of%20images%20being%20taken](https://www.nhs.uk/conditions/mri-scan/what-happens/#:~:text=A%20magnetic%20resonance%20imaging%20(MRI,number%20of%20images%20being%20taken). (accessed Sep. 20, 2023).
- [3] "Hr4 nanomotion motor ," NANOMOTION, <https://www.nanomotion.com/product/hr4-nanomotion-motor/> (accessed Sep. 20, 2023).
- [4] A. Sahu, H. Vikas, and N. Sharma, "Life cycle costing of MRI machine at a tertiary care teaching hospital," *The Indian journal of radiology & imaging*, <https://www.ncbi.nlm.nih.gov/pmc/articles/PMC7546299/> (accessed Sep. 20, 2023).
- [5] K. Albus, "Small phantom testing: MRI (revised 3-6-23)," Accreditation Support, <https://accreditationsupport.acr.org/support/solutions/articles/11000061036-small-phantom-testing-mri-revised-3-6-23-> (accessed Sep. 21, 2023).
- [6] "Liver Phantom — The Phantom Laboratory." <https://www.phantomlab.com/liver-phantom> (accessed Sep. 22, 2023).
- [7] J. Nofiele *et al.*, "An MRI-Compatible Platform for One-Dimensional Motion Management Studies in MRI," *Magnetic resonance in medicine*, vol. 76, no. 2, p. 702, Aug. 2016, doi: [10.1002/mrm.25903](https://doi.org/10.1002/mrm.25903).
- [8] Center for Devices and Radiological Health. "MRI Information for Industry." U.S. Food and Drug Administration, FDA, [www.fda.gov/radiation-emitting-products/mri-magnetic-resonance-imaging/mri-information-in-industry](http://www.fda.gov/radiation-emitting-products/mri-magnetic-resonance-imaging/mri-information-in-industry). Accessed 20 Sept. 2023.
- [9] "Motion Stages Compatible with CT, MRI, PET, SPECT & Ultrasound." <https://www.simutec.com/Products/motionstages.html> (accessed Sep. 20, 2023).

[10] "QUASAR™ MRI<sup>4D</sup> Motion Phantom," *Modus Medical Devices*.  
<https://modusqa.com/products/quasar-mri4d-motion-phantom/> (accessed Sep. 20, 2023).

## B. Preliminary Design Matrix

### MRI Compatible Motion Platform - BME 400

*Design Matrix*

February 27th, 2024

**Client:** Mr. Jiayi Tang

**Advisor:** Dr. James Trevathan

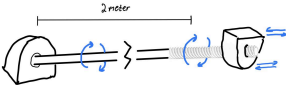
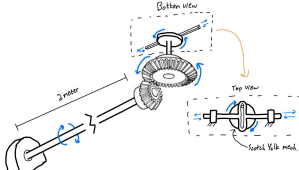
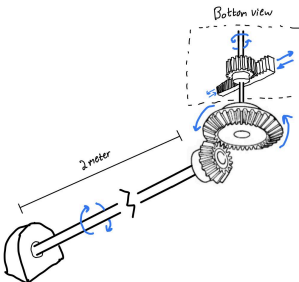
**Team:** Maxwell Naslund - Team Leader  
 Kendra Besser - Communicator  
 Amber Schneider - BWIG  
 Jamie Flogel - BPAG  
 Caspar Uy - BSAC

### Prototypes

**Design 1: Lead Screw**

**Design 2: Scotch Yoke**

**Design 3: Rack & Pinion**

Categories	Lead Screw	Scotch Yoke	Rack & Pinion
			

Efficiency (25)	2/5	10	4/5	20	5/5	25
Accuracy (20)	5/5	20	3/5	12	4/5	16
Ease of Fabrication (15)	2/5	12	4/5	12	3/5	12
Cost (15)	4/5	12	3/5	9	2/5	6
Adjustability (10)	5/5	10	2/5	4	4/5	8
Safety (10)	4/5	8	2/5	4	4/5	8
Durability (5)	1/5	1	4/5	4	4/5	4
Total (100)		73		65		79

### Design Criteria

- **Efficiency (25)**
  - The percent of power translated from rotational to linear motion
    - 97% for Rack & Pinion, 20-80% Lead Screw, 75% Scotch Yoke
- **Accuracy (20)**
  - How precise can the movement be within 1 waveform?
    - Lead screw limited by pitch
    - Scotch Yoke limited by length of the yoke
    - Rack and Pinion limited by gear teeth width
- **Ease of Fabrication (15)**
  - Off-the-shelf, non-complex, easy to assemble
    - We would have to printer a screw vertically so we are limited by size and availability of 3D printers
    - Rack and pinion requires a higher degree of precision when printing than the Scotch and Yoke design
- **Cost (15)**
  - Materials, fabrication, supporting pieces, both amount of materials and cost of materials
    - Lead screw requires the least material/least amount of parts
    - Rack and pinion requires the most amount of material
- **Adjustability (10)**
  - How adjustable is the design between different waveforms?
    - Lead screw can best adapt to different waveform
    - Would be less convenient to have to change out scotch yoke piece with different radii for different amounts of motion
- **Safety (10)**
  - Exposed moving pieces? The ability for the system to be MR-compatible

and prevent user injury

- Scotch yoke requires motion in multiple directions which poses the biggest potential safety concern

- **Durability (5)**

- Evaluates the device's wear proportionally to its time in use.
  - Lead screw has a higher wear rate than the other designs
  - Ball bearing reduces wear rate on the Scotch Yoke design

## C. Materials Expense Table

Item	Description	Manufacturer	Part Number	Date	QTY	Cost Each	Total	Link
<b>Component 1 - Gearbox Prints</b>								
Ultimaker PLA (118 g)	3D printed support for the driveshaft	Ultimaker	RAL-9005	11/17/2023	1	\$9.44	\$9.44	N/A
Ultimaker PLA (126 g)	3D printed gearbox extension pieces	Ultimaker	RAL-9005	2/27/2024	1	\$6.30	\$6.30	N/A
Ultimaker PLA	3D Printed Gears	Ultimaker	RAL-9005	3/7/2024	1	\$2.56	\$2.56	N/A
Ultimaker PLA	3D Printed Gearbox and motor stand	Ultimaker	RAL-9005	3/14/2024	1	\$19.60	\$19.60	N/A
<b>Component 2 - Linear Rails</b>								

Linear Rails	400 mm linear rails	igus	CWS-06-30-400	11/13/2023	2	\$167.69	\$335.38	<a href="#">Link</a>
<b>Component 3 - Linear Slides</b>								
Linear Slides	Slides to support platform on linear slides	igus	WWPL-06-30-06	11/13/2023	2	\$18.25	\$36.50	<a href="#">Link</a>
<b>Component 4 - Driveshaft</b>								
Driveshaft	Connection piece between motor and gearbox	Grainger	H0400075PW1000	11/16/2023	1	\$8.00	\$8.00	<a href="#">Link</a>
<b>Component 5 - Platform</b>								
Platform	1/4 black acrylic sheet provided by Makerspace	MSC	MSC# 63391700 (no part number given similar example)	11/17/2023	1	\$20.00	\$20.00	N/A
<b>Component 6 - Glass Ball Bearings</b>								
Glass Ball Bearings	Glass ball bearings to allow for frictionless rotation	Grainger	MSN0459939	12/1/2023	5	\$17.07	\$85.35	N/A

<b>Component 7 - Fasteners</b>								
M5 Plastic Screws	Used to assemble final prototype	Grainger	50M050080 H016	2/15/24	1	\$1.65 per package of 25	\$1.65	<a href="#">Link</a>
M4 Plastic Screws	Used to assemble final prototype	Grainger	50M040070N 035	2/15/24	2	\$5.92 per package of 25	\$11.84	<a href="#">Link</a>
Plastic Screws and Nuts	Plastic hardware from the makerspace	Makerspace	N/A	3/6/2024	1	\$1.30	\$1.30	N/A
<b>Component 8 Power Components</b>								
Power Inverter	Power supply inverter to improve circuit	DigiKey	PDM1-S5-D3 -S	3/22/2024	2	\$5.12	\$10.24	<a href="#">Link</a>
<b>Component 9 - unused features due to reprints/redesigns</b>								
Ultimaker PLA	3D printed Gearbox	Ultimaker	RAL-9005	10/26/2023	1	\$19.36	\$19.36	N/A
Ultimaker PLA	Motor to driveshaft adapter piece	Ultimaker	RAL-9005	12/1/2023	1	\$1.12	\$1.12	N/A



Ultimaker PLA	Motor to driveshaft adapter piece reprint	Ultimaker	RAL-9005	12/4/2023	1	\$2.84	\$2.84	N/A
Ultimaker PLA	Motor to driveshaft adapter piece reprint	Ultimaker	RAL-9005	12/5/2024	1	\$2.65	\$2.65	N/A
Ultimaker PLA (37.0 g)	3D printed gears to translate and facilitate motion	Ultimaker	RAL-9010	10/26/2023	1	\$2.96	\$2.96	N/A
Ultimaker PLA (325.0 g)	3D printed gears and gearbox	Ultimaker	RAL-9005	11/03/2023	1	\$26.00	\$26.00	N/A
Bamboo Labs PLA (127.34 g)	3D printed gearbox extension pieces	Bambu Lab	#000000	11/15/2023	1	\$12.19	\$12.19	N/A
Ultimaker PLA (27 g)	3D printed racks	Ultimaker	RAL-9005	11/29/2023	1	\$2.16	\$2.16	N/A
Ultimaker PLA (126 g)	3D printed Motor Stand	Ultimaker	RAL-9005	12/01/2023	1	\$10.08	\$10.08	N/A
Ultimaker PLA	3D printed gears and gearbox	Ultimaker	RAL-9005	2/23/24	1	\$14.60	\$14.60	N/A
<b>TOTAL:</b>	<b>\$642.12</b>							

## D. Fabrication Protocol

### Motor Assembly Copper Face

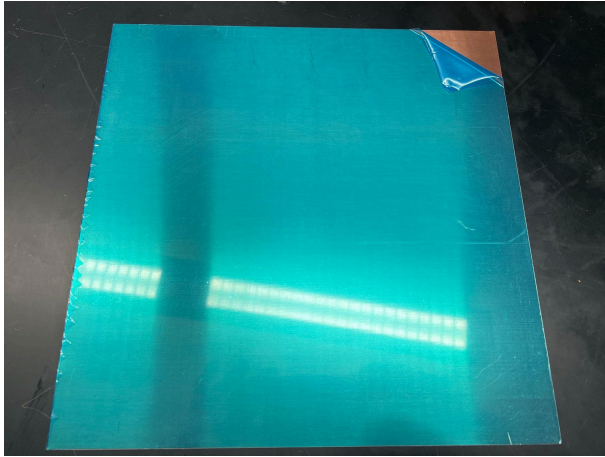


Figure 1: Uncut 1' x 1' copper sheet

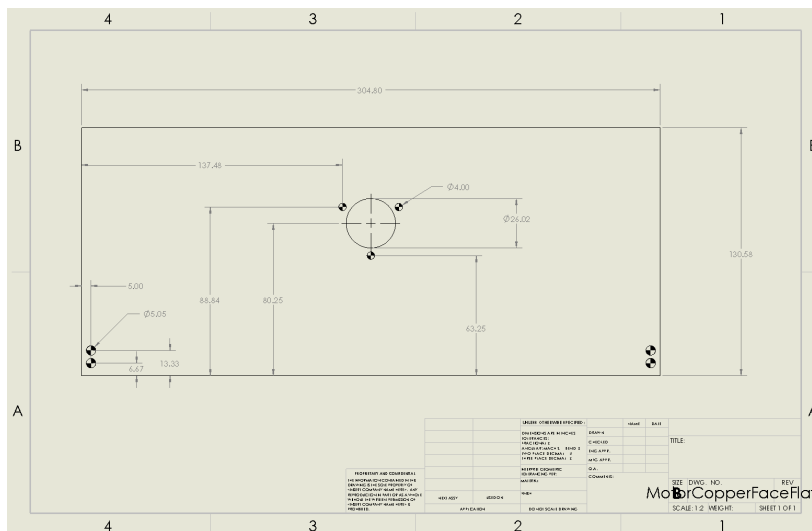


Figure 2: Copper face drawing

1. Starting from the 1' x 1' copper sheet illustrated in figure 1, on the metal shear in the TEAM Lab, cut a piece to 130.58cm tall.
2. Drill a pilot hole in the cut copper sheet at 152.4mm in the x-dimension, and 88.84mm in the y-direction as illustrated in figure 2.
3. Using a 1" hole saw, drill a 1" hole centered at the previously drilled pilot hole.
4. Drill three 3mm holes 120 degrees apart around the previously drilled 1" hole as illustrated in figure 2.
5. Drill four 5mm holes at the locations illustrated in figure 2.

### Motor Stand

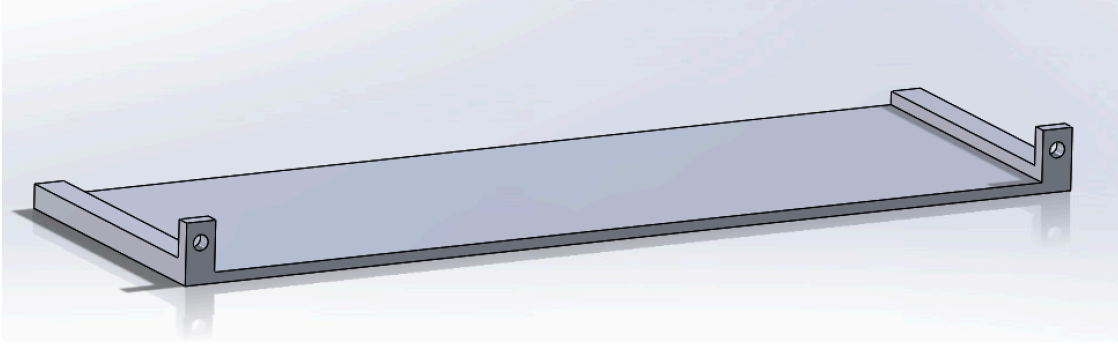


Figure 3: Motor stand SOLIDWORKS

1. 3D print attached motor stand .stl file at the Makerspace with 20% infill.

### Motor to Driveshaft Adapter

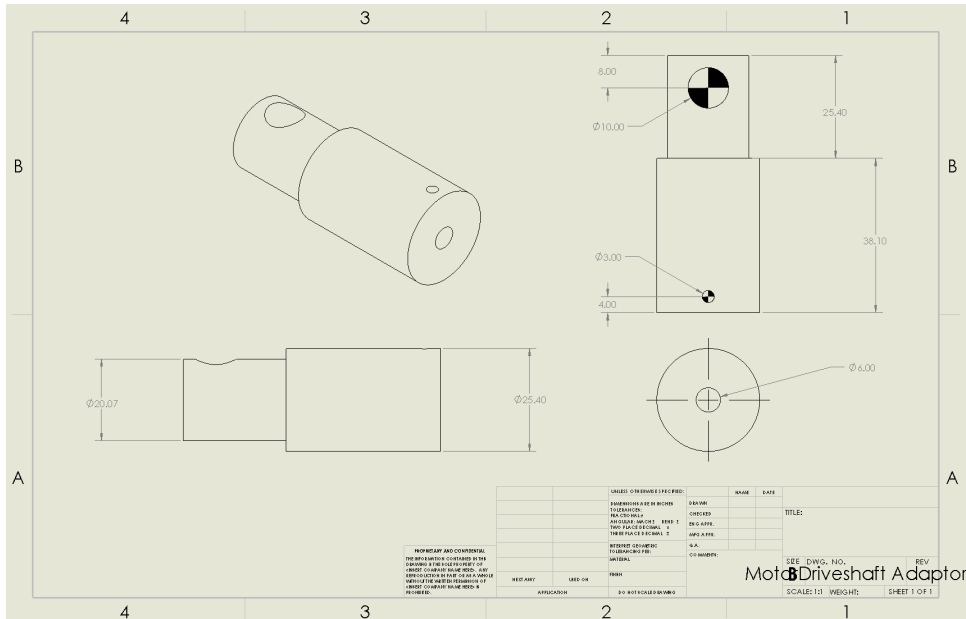


Figure 4: Driveshaft to Driveshaft Adapter drawing

1. Starting from 1" cylindrical aluminum stock, lathe one side down to a 20.07mm diameter 25.4mm in the TEAM Lab, as illustrated in figure 4.
2. Using a 6mm bit, drill a center hole 19mm deep on the side of the stock that is 25.4mm, as illustrated on figure 4.
3. Part the cylindrical aluminum stock off at 63.5mm, as illustrated in figure 4.
4. On the mill, drill a 3mm hole 4mm from the end of the 25.4mm end of the part. Drill down to the center hole drilled on the lathe, as illustrated on figure 4.
5. On the mill, drill a 10mm hole 8mm from the end of the 20.07mm end of the part. Drill all the way through the part, as illustrated on figure 4.

### Full Motor Assembly

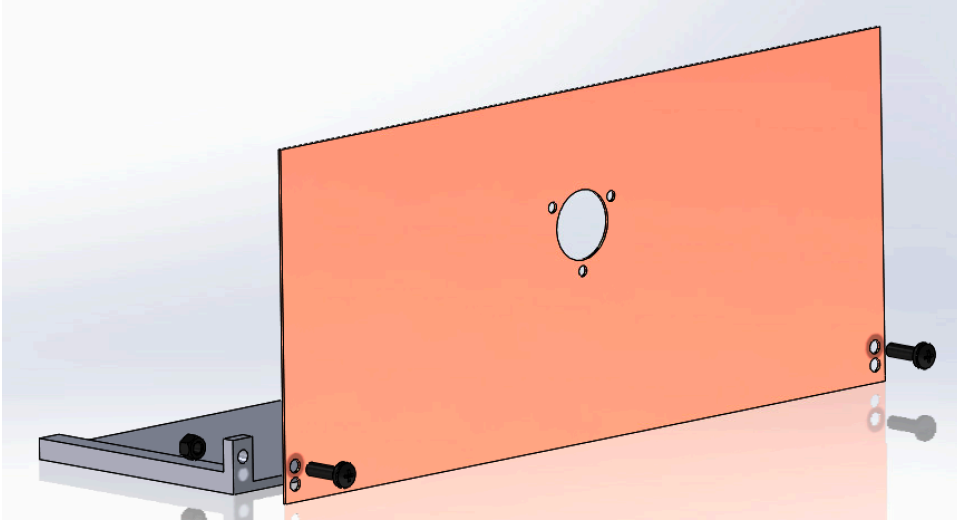


Figure 5: Motor stand and Face connected via two M5 screws

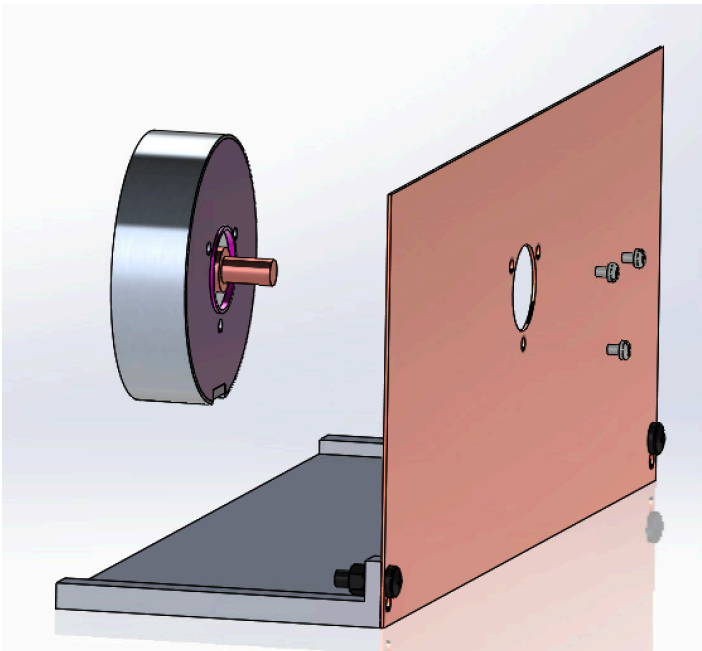


Figure 6: Motor connected to Motor stand via three M4 screws

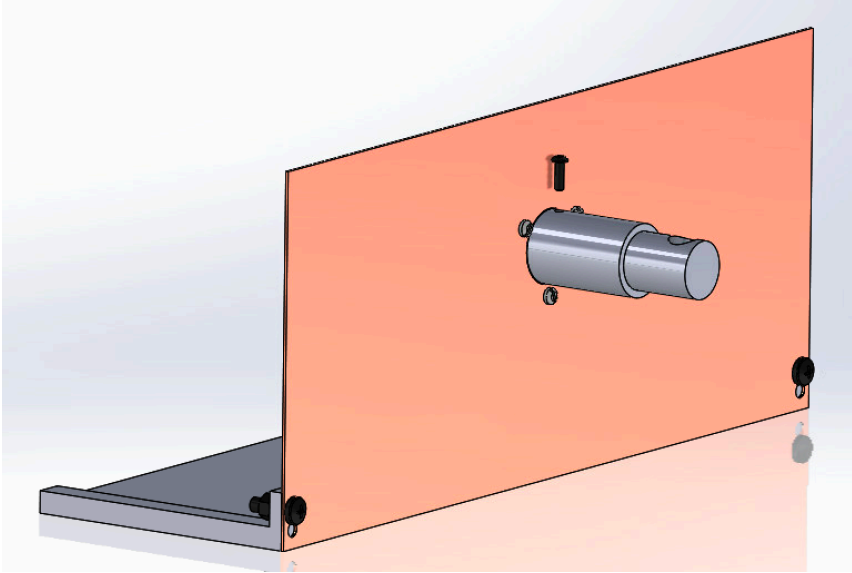


Figure 7: Motor to Driveshaft Adapter connected to motor via a M3 set screw

1. Using two M5 screws, attach copper face to copper stand. One screw on each side staggered, as illustrated in figure 5.
2. Using three M4 and three M4 washers, connect the piezoelectric motor to the copper face. Motor cable connection should point down, as illustrated in figure 6.
3. Slide the Motor to Driveshaft Adapter over the motor stud. Using a M3 screw, screw down onto one of the two flat sides of the motor stud to secure the adapter to the motor, as illustrated in figure 7.

## Gearbox Assembly

### 3D Print Components

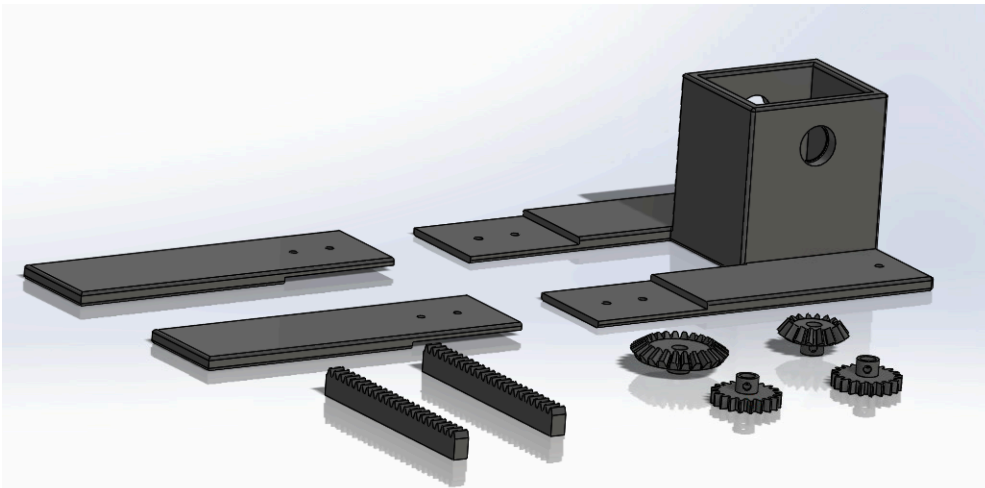


Figure 8: Gearbox 3D printed components

At the Makerspace, 3D print the Gearbox, Gearbox Extensions, Bevel Gears, Pinion Gears, and Rack Gears at 20% infill, as illustrated in figure 8.

## Crosspin

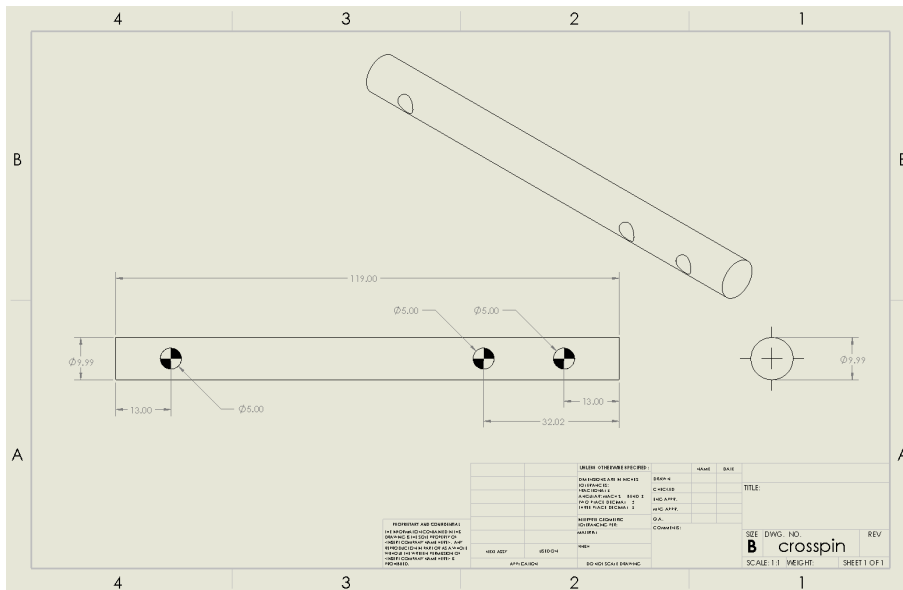


Figure 9: Crosspin drawing

1. In the TEAM Lab, start with 1" HDPE cylindrical stock. Lathe the piece down to 10mm diameter.
2. Using a 5mm bit, on the mill drill three holes in the crosspin in the locations illustrated in figure 9.

## Gearbox to Driveshaft Adapter

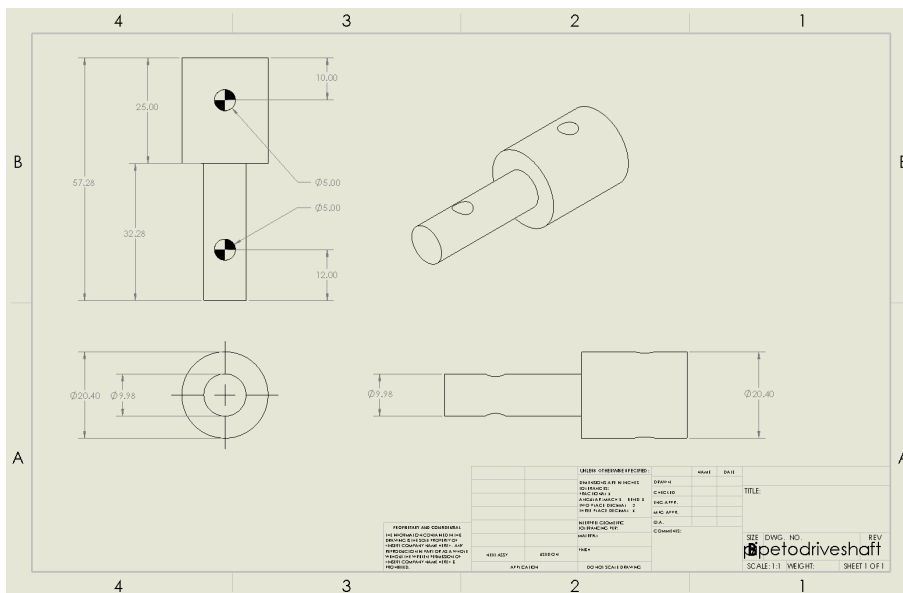


Figure 10: Gearbox to Driveshaft Adapter



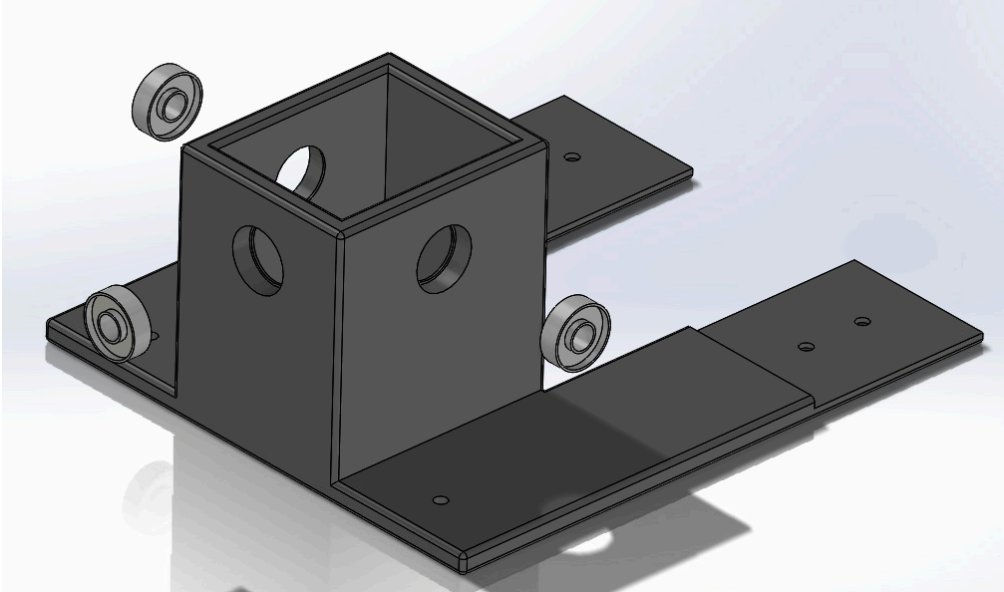


Figure 12: Adding bearings to gearbox

1. Insert three glass ball bearings into the gearbox as illustrated in figure 12.

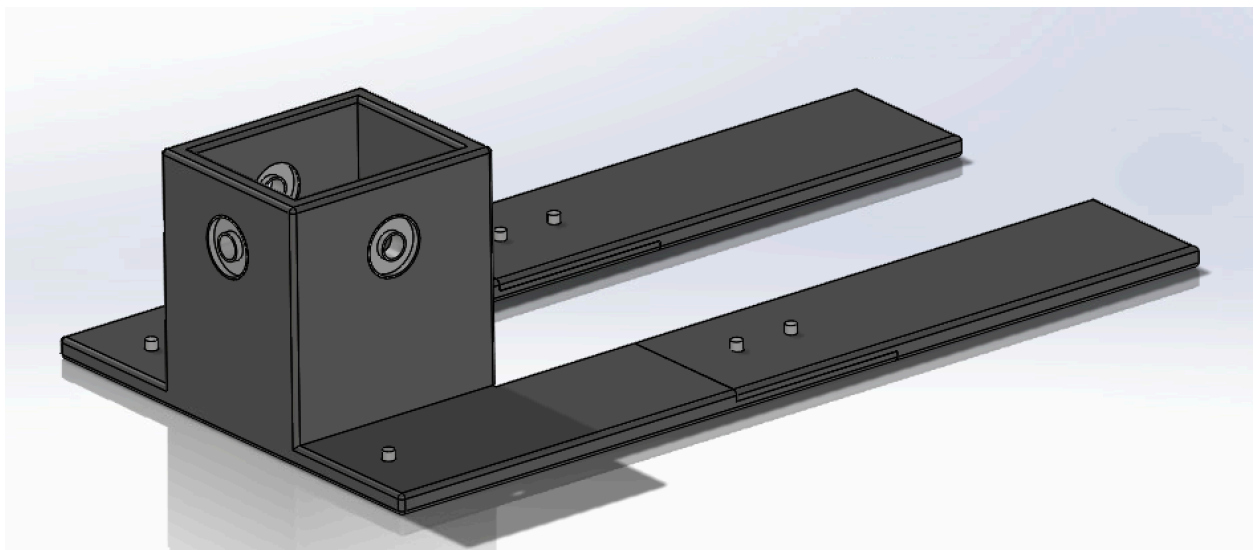


Figure 13: Adding Gearbox extensions

2. Connect 3D printed gearbox extension pieces to the gearbox via six M5 screws, as shown in figure 13. Screws should be screwed in from the bottom up.



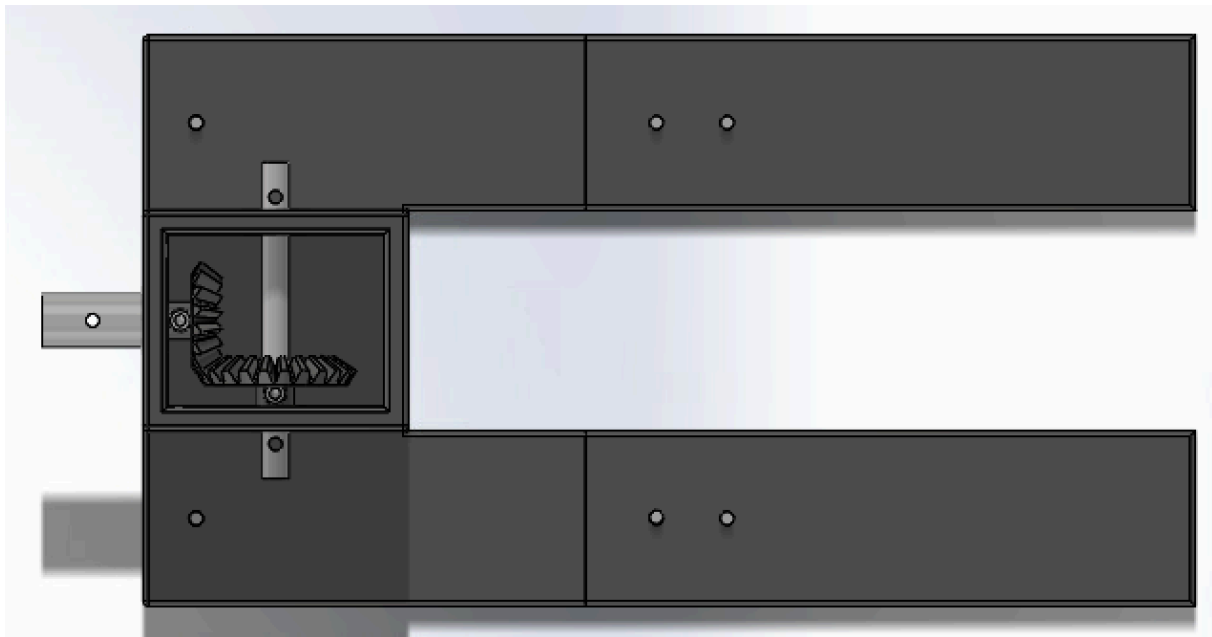


Figure 14: Adding internal components to gearbox

3. Add Gearbox to Driveshaft adapter, Crosspin, and bevel gears in the configuration illustrated in figure 14.
4. Using two M5 screws, anchor the bevel gears to the crosspin and adapter.

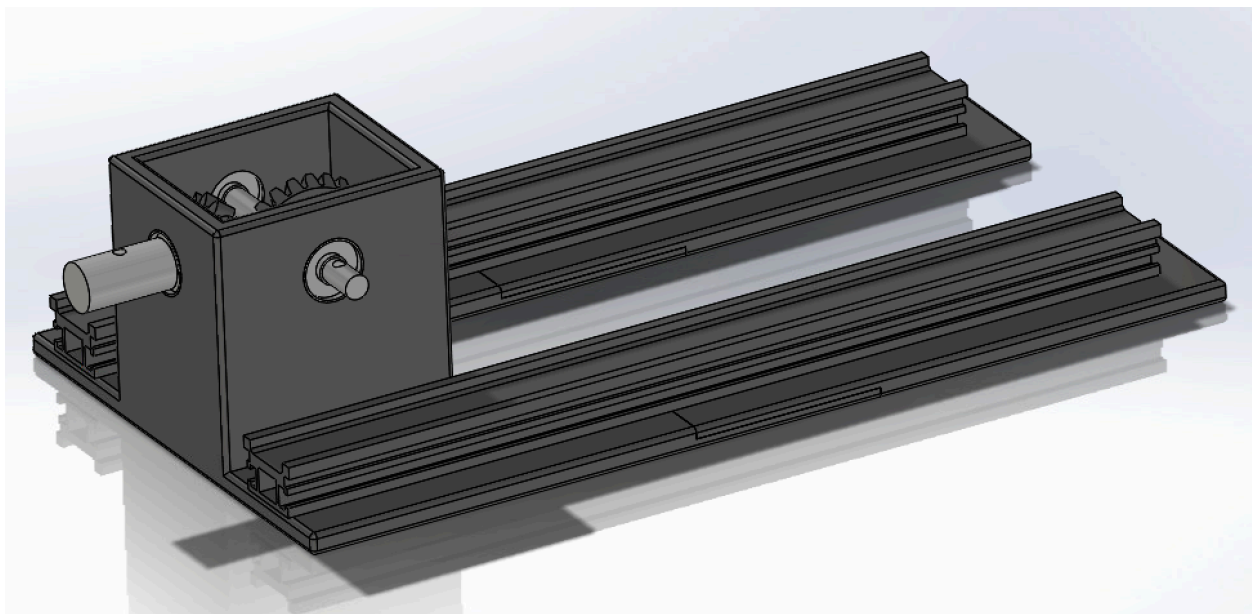


Figure 15: Adding linear rails to assembly

- Using the same six M5 screws to connect the gearbox to the gearbox extensions, connect two linear rails as illustrated in figure 15.



Figure 16: Adding linear slides to assembly

- Using eight M4 screws, attach two linear slides to the bottom of the phantom bed as illustrated in figure 16.

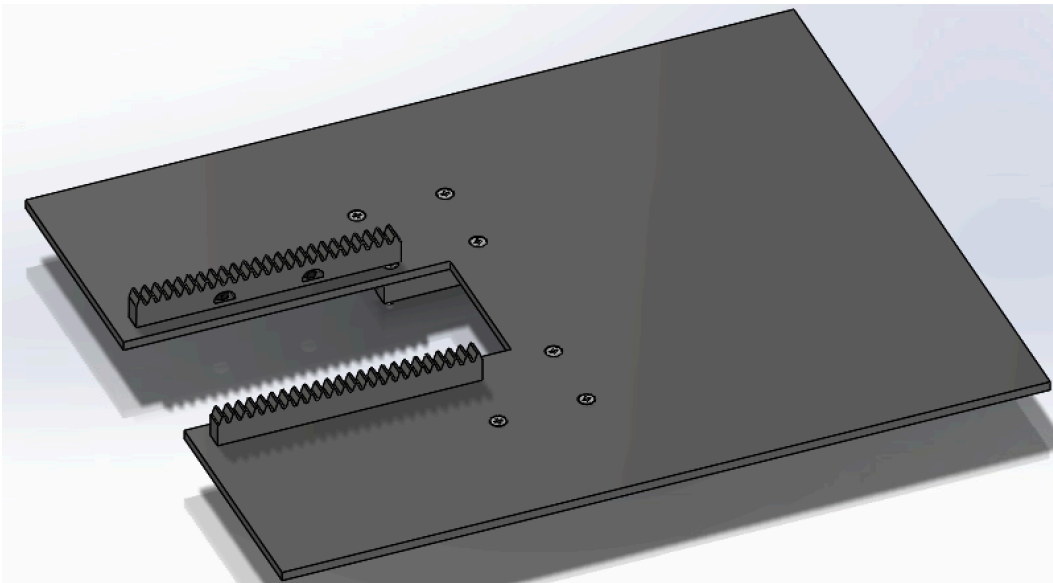


Figure 17: Adding rails to phantom bed

- Using four M4 screws and nuts (two per rail) attach rails to the phantom bed as illustrated in figure 17.

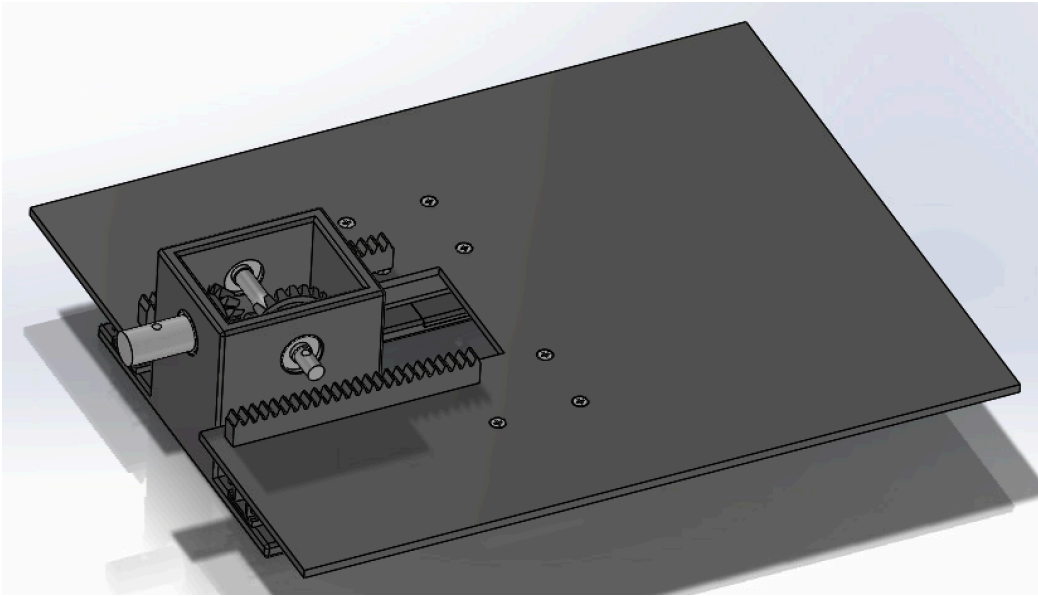


Figure 18: Adding phantom bed to gearbox

8. Slide the linear slides on the bottom of the phantom bed on top of the linear rails attached to the gearbox as illustrated in figure 18.

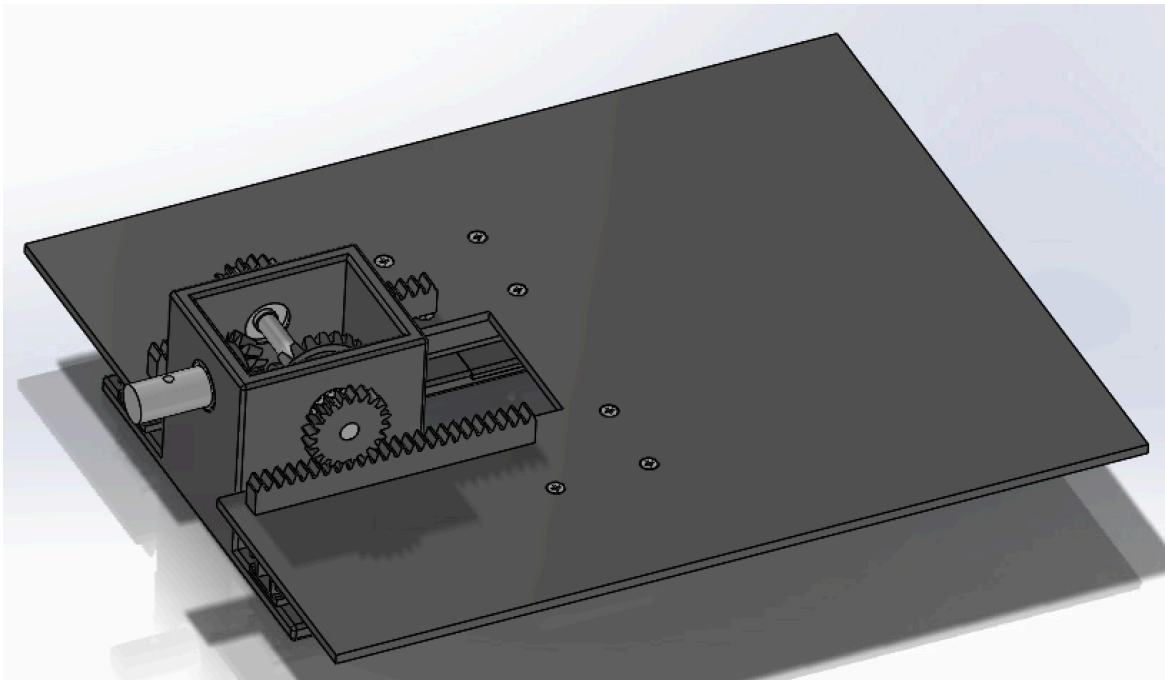


Figure 19: Adding pinion gears to assembly

9. Slide pinion gears onto both sides of the crosspin as shown in figure 19.
10. Using two M5 screws, anchor pinion gears to crosspin.

## Driveshaft

1. Cut a 10' long  $\frac{3}{4}$ " pvc pipe into two pieces. One measuring 4' and the other 6'. Only the 4' long pieces will be used in the full prototype assembly.
2. In the TEAM Lab, using a drill press, drill a 10mm hole 8mm from one end of the pipe.
3. Using a drill press, drill a 5mm hole 10mm from the other end of the pipe.

## Full Prototype Assembly

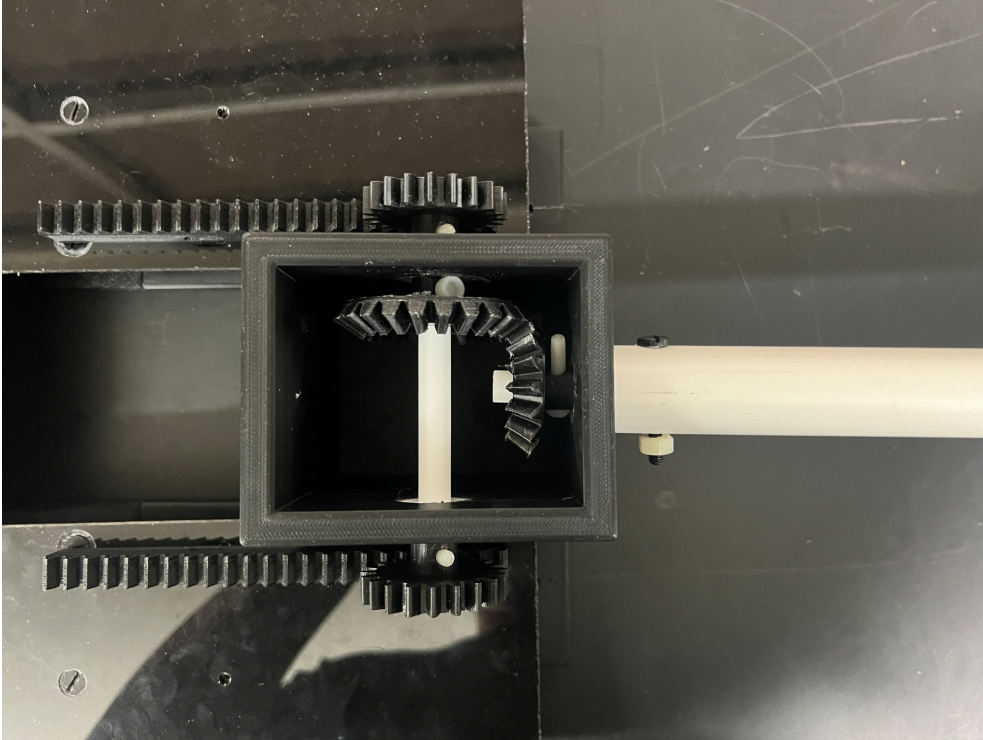


Figure 20: Attaching driveshaft to gearbox

1. Connect one side of the 4' driveshaft to the gearbox to driveshaft adapter via a M5 screw.

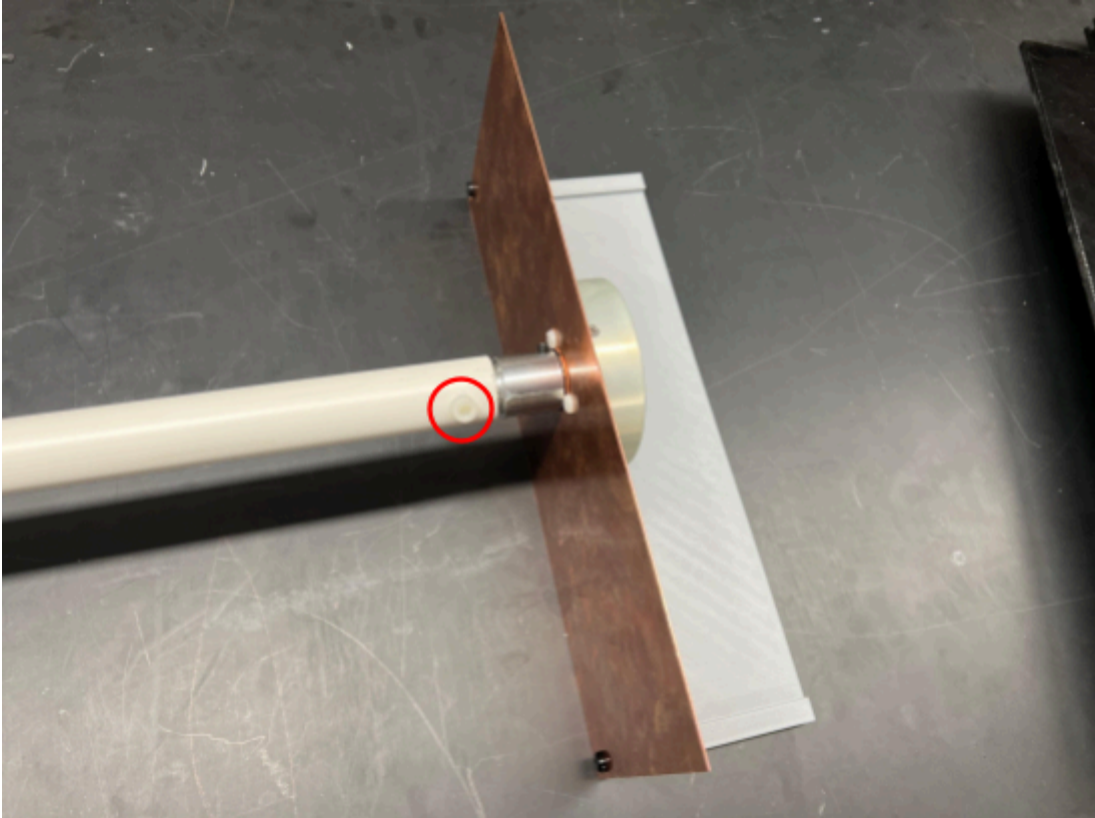


Figure 21: Attaching driveshaft to Motor assembly

2. Connect the other side of the 4' driveshaft to motor assembly via a M10 screw and nut as illustrated in figure 21.



Figure 22: Full prototype assembly

3. Full prototype has been completed.